Inorganic Chemistry

Article

pubs.acs.org/IC

Magnetic Circular Dichroism Spectrum of the Molybdenum(V) Complex [Mo(O)Cl_3dppe]: *C*-Term Signs and Intensities for Multideterminant Excited Doublet States

Anne Westphal,[†] Henning Broda,[†] Philipp Kurz,[†] Frank Neese,[‡] and Felix Tuczek*,[†]

[†]Institut für Anorganische Chemie, Christian-Albrechts-Universität zu Kiel, D-24118 Kiel, Germany

[‡]Max-Planck-Institut für Bioanorganische Chemie, D-45470 Mülheim an der Ruhr, Germany

Supporting Information

ABSTRACT: The molybdenum(V) complex [Mo(O)-Cl_3dppe] [dppe = 1,2-bis(diphenylphosphino)ethane] is considered as a model system for a combined study of the electronic structure using UV/vis absorption and magnetic circular dichroism (MCD) spectroscopy. In order to determine the signs and MCD *C*-term intensities of the chlorido → molybdenum charge-transfer transitions, it is necessary to take the splitting of the excited doublet states into sing-doublet and trip-doublet states into account. While transitions to the sing-doublet states are electric-dipole-allowed, those to the trip-doublet states are electric-dipole-forbidden. As spin−orbit coupling within the manifold of sing-doublet states vanishes, configuration interaction between the sing-doublet and trip-doublet states is required to generate the MCD *C*-term intensity. The most prominent feature in the MCD spectrum of [Mo(O)Cl_3dppe] is a "double *pseudo-A* term", which consists of two corresponding *pseudo-A* terms centered at 27000 and 32500 cm^{-1}. These are assigned to the ligand-to-metal charge-transfer transitions from the p_π orbitals of the equatorial chlorido ligands to the Mo d_{yz} and d_{xz} orbitals. On the basis of the theoretical expressions developed by Neese and Solomon (*Inorg. Chem.* **1999**, *38*, 1847−1865), a general treatment of the MCD *C*-term intensity of these transitions is presented that explicitly considers the multideterminant character of the excited states. The individual MCD signs are determined from the corresponding transition densities derived from the calculated molecular orbitals of the title complex (BP86/LANL2DZ).

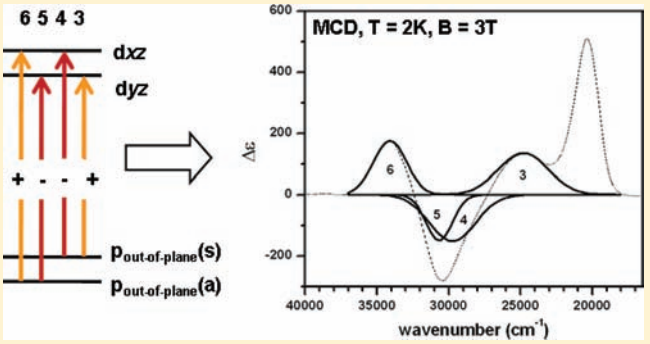

INTRODUCTION

Magnetic circular dichroism (MCD) spectroscopy is a powerful tool to gain insight into the electronic structures of transition-metal complexes. In MCD spectroscopy, the differential absorption $\Delta\varepsilon$ between left (lcp) and right (rcp) circularly polarized light of a sample is measured in the presence of a longitudinal magnetic field.[1−14] Because $\Delta\varepsilon$ can be positive or negative, the observed MCD transitions exhibit positive or negative signs. This property renders MCD complementary (and potentially superior) to ordinary electronic absorption spectroscopy, where only (intrinsically positive) absorption intensities are measured.

Three different mechanisms contribute to the intensity of a MCD signal, designated as *A*-, *B*-, and *C*- terms.[15,16] While the *A*-term intensity arises from the splitting of a degenerate excited state in the presence of an external magnetic field and shows a derivative band shape, the *C*-term intensity is observed as a consequence of the splitting of a degenerate ground state. A third contribution, the *B*-term intensity, arises from the coupling of two formerly independent excited states in the presence of an external magnetic field. Like the MCD *C*-term mechanism, it gives rise to an usual absorption band shape. In contrast to the *A*- and *B*-term intensities, the MCD *C*-term intensity is temperature-dependent ($\sim 1/T$) and thus dominates the MCD spectrum at very low temperatures.

From variable temperature and variable field (VTVH) measurements of the *C*-term intensity, characteristic ground-state properties including *g* values, zero-field-splitting parameters and coupling constants, and polarization of the individual transitions can be obtained.[1,17] In many cases, MCD spectroscopy is only used to gain ground-state information, and the individual transitions are assigned without accounting for the positive and negative signs of the MCD (*C*-term) intensities.[3−8,10−14] Determination of the MCD signs is, in fact, not trivial, but being neglected leads to an incomplete utilization of the potential of this method, a loss of spectral information with respect to the manifold of excited states, and the possibility of erroneous band assignments.

In the limit of a pure *C*-term mechanism, the MCD intensity is given by

$$\frac{\Delta\varepsilon}{E} = \frac{\varepsilon_{lcp} - \varepsilon_{rcp}}{E} = \frac{\gamma\beta_B B}{kT}\bar{C}_0 f(E)$$

Received: January 27, 2012
Published: May 1, 2012

   dx.doi.org/10.1021/ic300201t | *Inorg. Chem.* 2012, 51, 5748−5763

Scheme 1. (Left) "*J*–*K* Coupling" Mechanism Gives Rise to a Nonzero MCD *C*-Term Intensity If Two Excited States, *J* and *K*, Interact via Spin–Orbit Coupling and the Individual Transitions $A \rightarrow J$ and $A \rightarrow K$ Are Polarized in Different Directions Perpendicular to the Spin–Orbit Coupling Vector; (Right) Origin of a So-called "Double *Pseudo-A* Term"

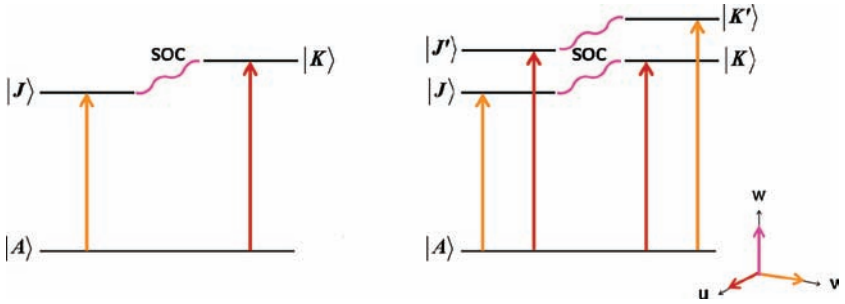

where γ is a collection of constants, β_B is the Bohr magneton, k is the Boltzmann constant, T is the absolute temperature, B is the magnetic flux density, and $f(E)$ is a line-shape function. Here, it is sufficient to consider $f(E)$ as a δ function and E as the transition energy. After orientational averaging, the C_0 parameter results as

$$\bar{C}_0 = -\frac{1}{6}(M_{yz}^{\mathrm{eff}} g_x + M_{zx}^{\mathrm{eff}} g_y + M_{xy}^{\mathrm{eff}} g_z)$$

where g_u are the components of the ground-state **g** tensor (u = x, y, and z) and M_{vw}^{eff} are effective transition-dipole moments (vw = xy, zx, and yz), which are given by

$$M_{vw}^{\mathrm{eff}} = \sum_{K \neq A,J} (\vec{D}_v^{AK} \vec{D}_w^{AJ} - \vec{D}_w^{AK} \vec{D}_v^{AJ}) \frac{\bar{L}_u^{KJ}}{\Delta_{KJ}} + (\vec{D}_v^{AJ} \vec{D}_w^{JK} - \vec{D}_w^{AJ} \vec{D}_v^{JK}) \frac{\bar{L}_u^{KA}}{\Delta_{KA}}$$

The states A, J, and K are given as eigenfunctions of S and M_S; i.e., $A = |ASM_S\rangle$, etc. The transition-dipole matrix elements $\vec{D}_u^{AB}$ are defined as

$$\vec{D}_u^{AB} = \langle ASM_S|\mu_u|BSM_S\rangle$$

and the reduced spin–orbit coupling matrix elements $\bar{L}_u^{AB}$ are defined as

$$\bar{L}_u^{AB} = \mathrm{Im}\langle ASS| \sum_i h_u(i)\, s_0(i)|BSS\rangle_0$$

where $s_0(i)$ is the s_z component of the spin operator acting on the ith electron and the sum runs over all electrons i. In this expression, the operator $h_u(i)$ is given by

$$h_u(i) = \sum_N \xi(r_{iN})\, l_{N,u}(i)$$

where N denotes the atom and ξ is the spin–orbit coupling constant. $l_{N,u}(i)$ is the uth component of the orbital angular momentum operator acting on electron i relative to nucleus N. Spin–orbit coupling is usually only considered within the metal atom.

The above equations indicate that the MCD *C*-term intensity may arise through spin–orbit coupling between the excited states J and K ($A \rightarrow J$, $A \rightarrow K$, with J and K being coupled through spin–orbit coupling, "*J*–*K* coupling") or between ground state A and excited state K ($A \rightarrow J$, $K \rightarrow J$, with A and K being coupled through spin–orbit coupling, "*A*–*K* coupling"). Considering the "*J*–*K* coupling" mechanism, the individual transitions $A \rightarrow J$ and $A \rightarrow K$ must be polarized in different directions perpendicular to the spin–orbit coupling vector to result in nonzero *C*-term intensities (Scheme 1, left).[1]

If both transitions are observed in the MCD spectra, they show opposite signs and, given that the excited-state splitting is comparable to the bandwidth, may appear as one derivative-shaped band, which is then called a *pseudo-A* term. The absolute signs of the $A \rightarrow J$ and $A \rightarrow K$ transitions generally depend on the symmetry of the considered states, i.e., on the symmetry of the involved molecular orbitals (MOs).

MCD *C*-term transitions between a pair of (almost) degenerate donor orbitals and a pair of (almost) degenerate acceptor orbitals of appropriate symmetry may result in two oppositely signed *pseudo-A* terms of equal intensity, which is then called a "double *pseudo-A* term" (Scheme 1, right). Consisting of four related MCD bands, this spectral feature shows a characteristic band pattern of positive–negative–negative–positive or negative–positive–positive–negative intensities, depending on the particular symmetries of the involved orbitals.

A general quantum-mechanical formalism to calculate the signs and intensities of MCD *C*-term transitions for spins $\geq {}^1/_2$ has been presented by Neese and Solomon.[1] The theory has been formulated in terms of the eigenstates of the Born–Oppenheimer Hamiltonian. Such extremely complex wave functions cannot be determined in practice. The most general computational realization of the concept involves elaborate multireference configuration interaction (CI) wave functions.[18] However, it is somewhat limited in its applicability because of the high computational cost of the multireference treatment.[19] In order to obtain chemical insight, simpler equations have been derived from the general treatment in terms of single-determinant excited-state configuration-state functions (CSFs). However, only a few classes of excitations were considered in the original treatment, which are (i) transitions from doubly occupied MOs into singly occupied MOs (SOMOs; type I) and (ii) transitions from SOMOs into unoccupied MOs (type II). To the best of our knowledge, no qualitative and experimentally verified theoretical treatment of *C*-term transitions exists so far for the case of (iii) transitions from doubly occupied MOs to unoccupied MOs (type III), which generally applies to all ligand-to-metal charge transfer (LMCT) into unoccupied metal d orbitals as well as to metal-to-ligand charge transfer (MLCT) from doubly occupied metal d orbitals to unoccupied ligand MOs. In both cases, multideterminant wave functions are needed to correctly describe the considered excited states.[20] It is the purpose of the present paper to explicitly consider these types of electronic transitions on the basis of the most simple example, a transition-metal d^1 complex. Obviously, this system gives rise to type I–III electronic transitions

dx.doi.org/10.1021/ic300201t | Inorg. Chem. 2012, 51, 5748–5763

(Scheme 2). While the $S = {}^1/_2$ ground states and $S = {}^1/_2$ excited states involved in the type I and II transitions can be represented

Scheme 2. Type I–III Electronic Transitions in $S = {}^1/_2$ Systems (Only $M_S = +{}^1/_2$ Ground- and Excited-State Configurations Are Shown)

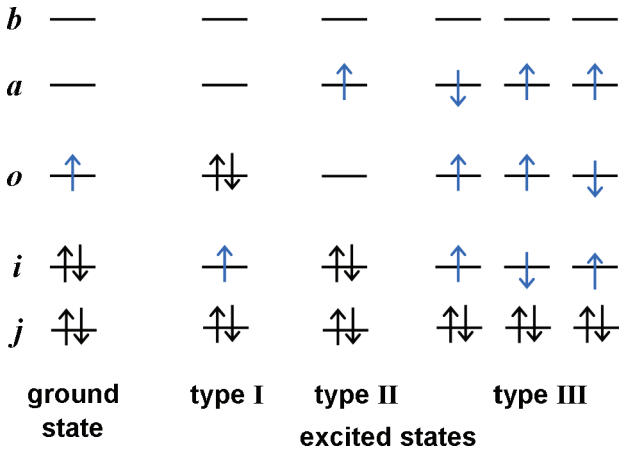

by single determinants, the excited doublet states of type III transitions split into sing-doublet and trip-doublet states. It will be described how this situation can be treated theoretically to derive the signs and intensities of the corresponding *C*-term transitions.

In the present study, we focus on the molybdenum(V) (d^1) complex [Mo(O)Cl_3dppe] [dppe = 1,2-bis(diphenylphosphino)-ethane]. Molybdenum oxido–halogenido complexes with phosphine coligands are important precursors for molybdenum dinitrogen complexes.[21,22] The MCD spectra of the pseudo-C_S-symmetric [Mo(O)X_2L] complexes [L = hydrotris(3,5-dimethyl-1-pyrazolyl)borate; X = O (diol, chatecholato), Cl, or S (dithiolato)] have been investigated previously.[2] The observed bands were assigned according to a rule that states that transitions between two electronic states with different symmetries (a′ → a″) result in positive-signed MCD bands, while negative signs are obtained if no change of symmetry is involved (a′ → a′ and a″ → a″). In the present paper, we will develop a more general treatment that does not rely on the symmetry properties of the complex under investigation and, in addition, allows one to calculate the intensities of the MCD *C*-term transitions on the basis of the theoretical expressions presented earlier.[1] The signs of the *C*-term transitions will be directly derived from the MO scheme obtained by density functional theory (DFT). Ziegler and co-workers have assigned the MCD spectra of several molybdenum(V) complexes based on time-dependent DFT (TDDFT) calculations of the MCD *C*-term intensities and signs,[23] employing the approach of magnetic perturbation theory.[24] However, the subtle "trip-doublet"-type spin coupling that is important for properly treating type III excitations is not correctly represented in a TDDFT (or any self-consistent field like linear response) treatment because determinants that are double excited in terms of spin orbitals are necessary to obtain the excited CSFs of correct spin multiplicity. This is the subject of the present paper.

To exemplify the application of the described protocol, UV/vis and low-temperature MCD spectra of the complex [Mo(O)Cl_3dppe] are measured in a CH_2Cl_2 solution and CH_2Cl_2/polystyrene films, respectively. Electronic transitions are assigned on the basis of DFT and TDDFT calculations. Then, theoretical expressions for the MCD *C*-term intensities of type III electronic transitions are developed that allow calculation of the intensities of the observed spectroscopic features. The corresponding MCD signs are determined from the calculated MO scheme and the derived transition densities. Complementary information is derived from IR and Raman spectroscopy, leading to a much advanced understanding of the electronic and vibrational structures of the title complex.

EXPERIMENTAL SECTION

[Mo(O)Cl_3dppe] was synthesized using common Schlenk techniques (N_2). Sample preparation was always carried out under a N_2 atmosphere.

Synthesis. [Mo(O)Cl_3dppe] [dppe = 1,2-bis(diphenylphosphino)-ethane] was synthesized according to a previously reported literature procedure[25] and obtained as a red crystalline powder in a yield of 43%. The purity of the obtained product was confirmed by elemental analysis [found (calcd): C, 51.5 (51.6); H, 3.4 (3.9); Cl, 15.9 (17.3)].

Vibrational Spectra. The MIR spectrum of the solid sample was measured in KBr using a Bruker IFS v66/S Fourier transform infrared (FT-IR) spectrometer. The FT-Raman spectrum of the solid sample was recorded with a Bruker IFS 666/CS near-IR (NIR) FT-Raman spectrometer. A Nd:YAG laser with an excitation wavelength of 1064 nm was used as a light source. The resonance Raman spectrum was recorded with a DILOR XY-multichannel Raman spectrometer with a triple monochromator and a CCD detector. Excitation wavelengths between 454.5 and 647.1 nm were generated by an Ar^+/Kr^+ laser.

UV/Vis Absorption Spectra. The UV/vis absorption spectra of 1 and 0.1 mM solutions of the title complex in CH_2Cl_2 were recorded at room temperature with a Cary 5000 NIR spectrometer using quartz cuvettes (path length d = 10 mm).

MCD Spectra. Low-temperature MCD data were recorded at T = 2 K using a Jasco J810 CD spectropolarimeter associated with an Oxford SM 4000-9 magnetocryostat, as previously described.[10] Magnetic field strengths were varied between 0 and ±3 T. Thin polystyrene film samples were prepared by evaporation of a 1 mM dichloromethane complex solution containing a sufficient amount of polystyrene. After subtraction of the B = 0 T reference spectrum, the resulting MCD spectra were deconvoluted by Gaussian curve fits to resolve the individual transitions.

Computational Details. Spin-unrestricted DFT calculations were performed using *Gaussian03*.[26] The B3LYP hybrid functional[27–29] was employed for geometry optimization of the complex structure, calculation of the vibrational spectra, and TDDFT calculation of the electronic transitions, while calculation of the MOs was done using the BP86 functional.[30–32] The LANL2DZ basis set was always used for all types of atoms.[33–36] The MOs were plotted with *Gabedit*.[37]

RESULTS AND DISCUSSION

Complex Structure and Vibrational Spectra. The optimized structure of [Mo(O)Cl_3dppe] shows a slightly distorted octahedral complex geometry of pseudo-C_S symmetry (Figure 1 and Table 1). The dppe ligand and two chlorine atoms are equatorially coordinated. The third chlorido ligand is found trans to the oxido group, with the Mo–Cl_{ax} metal–ligand bond length being elongated by 0.12 Å compared to the two Mo–Cl_{eq} distances. Because of the short ethylene bridge of the dppe ligand, the P–Mo–P angle is only 81°, resulting in a Cl_{eq}–Mo–Cl_{eq} angle that is significantly larger than 90°. The axial chlorido ligand and oxido group are significantly bent from the molecular z axis toward the dppe ligand with a Cl_{ax}–Mo–O angle of only 158°.

The vibrational spectra (MIR and FT-Raman) of [Mo(O)Cl_3dppe] (Figure 2) are dominated by the various phenyl C=C and C–H stretching and bending vibrations of the dppe ligand. However, the most characteristic vibrations are the metal–ligand stretches, which can be assigned with the help of

dx.doi.org/10.1021/ic300201t | Inorg. Chem. 2012, 51, 5748–5763

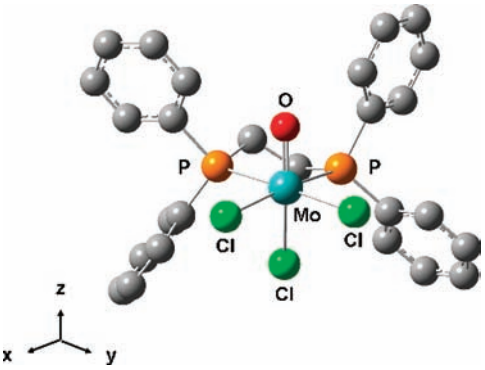

Figure 1. Optimized complex structure of [Mo(O)Cl_3dppe] obtained from a DFT geometry optimization (B3LYP/LANL2DZ). Hydrogen atoms are omitted for clarity.

Table 1. Metal–Ligand Bond Distances and Bond Angles of [Mo(O)Cl_3dppe] Obtained from a Quantum-Chemical Geometry Optimization (B3LYP/LANL2DZ)

bond distances (Å)		bond angles (deg)	
Mo–P	2.70/2.69	P–Mo–P	81
Mo–Cl_{eq}	2.41/2.41	Cl_{eq}–Mo–Cl_{eq}	97
Mo–Cl_{ax}	2.53	P–Mo–Cl_{eq}	90°/91
Mo–O	1.73	O–Mo–Cl_{ax}	158
		Cl_{eq}–P–P–Cl_{eq}	−3.4

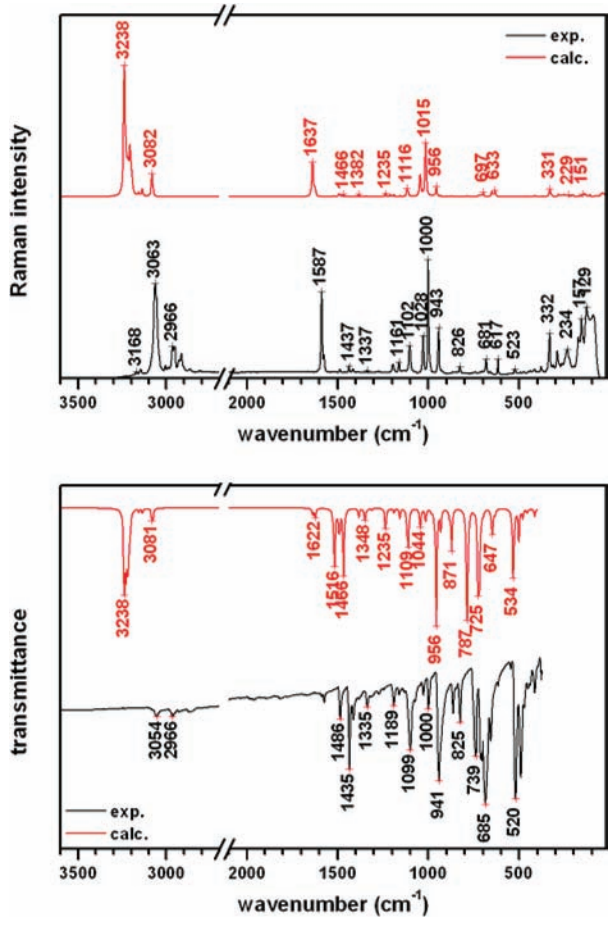

Figure 2. Experimental and calculated MIR and Raman spectra of [Mo(O)Cl_3dppe]. Theoretical spectra were computed by DFT calculations (B3LYP/LANL2DZ).

DFT calculations. The Mo–oxido stretching vibration (IR, 941 cm^{-1}; Raman, 943 cm^{-1}) and the Mo–P stretch (IR, 520 cm^{-1}) show very high intensities, especially in the IR spectra. The Mo–Cl stretching vibrations are observed in the Raman spectrum at 332 cm^{-1} (Mo–Cl_{eq}, symm) and 234 cm^{-1} (Mo–Cl_{ax}). An overview of the most intense vibrations is given in Table 2. The very good match between the experimental and the calculated IR and Raman spectra ensures the reliability of the optimized complex structure for its further use in the quantum-chemical calculations of MOs and electronic transitions.

Table 2. Overview of the Most Characteristic Vibrations of [Mo(O)Cl_3dppe]

IR (cm^{-1})		Raman (cm^{-1})		
expt	calcd	expt	calcd	assignment
	228	234	228	Mo–Cl_{ax} stretch
	331	332	331	Mo–Cl_{eq} stretch (symmetric)
491	502			C–P bending vibrations
520	534			Mo–P stretch
656	647	617	(630)	combined P–C_{en} stretch (symm + antisymm)
685–740	725, 787	681		C(–H)$_{phenyl}$, out-of-plane bending
941	956	943	956	Mo=O stretch
		1000	1015	(C=C)$_{phenyl}$, symmetric in-plane bending (ring breathing)
1028, 1099	1044, 1109	1028, 1102	1045, 1116	P–C_{Ph} stretch
1435, 1486	1466, 1516	1486	1493	C=C stretch (antisymmetric)
1572	1622	1587	1637	C=C stretch (symmetric)
3054	3238	3063	3238	C–H stretch (phenyl)

UV/Vis Absorption Spectra. The most prominent feature of the UV/vis spectrum of [Mo(O)Cl_3dppe] is the distinct absorption band B centered at 20500 cm^{-1} (ε = 2100 $Lmol^{-1}cm^{-1}$; Figure 3). This band shows a slight asymmetry, indicating that another band might additionally be hidden beneath at around 21500 cm^{-1} (band C). A UV/vis absorption band at around 20000 cm^{-1} has already been reported for

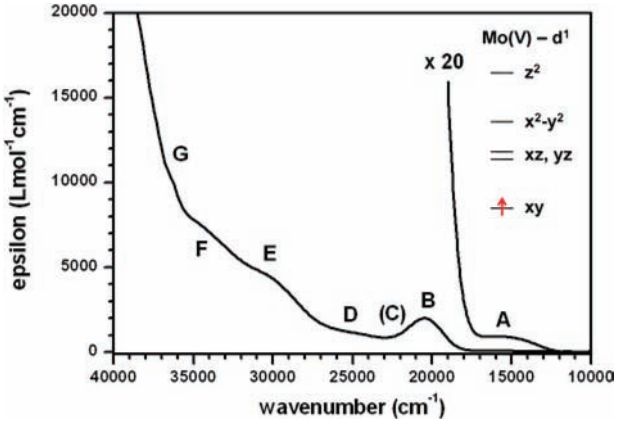

Figure 3. UV/vis absorption spectrum of [Mo(O)Cl_3dppe] measured in CH_2Cl_2 at room temperature. Inset: Schematic ligand-field splitting of the metal d orbitals for a distorted octahedral d^1 system. It is characteristic for the tetragonally compressed complex geometry of [Mo(O)Cl_3dppe].

dx.doi.org/10.1021/ic300201t | Inorg. Chem. 2012, 51, 5748–5763

[Mo(O)Cl_3dppe] and [Mo(O)Cl_3dppen] [dppen = 1,2-bis-(diphenylphosphino)ethene] and was assigned to the $d_{xy} \rightarrow d_{x^2-y^2}$ ligand-field transition.[38] In the case of the molybdenum(V) complex [Mo(O)Cl_2L] [L = hydrotris(3,5-dimethyl-1-pyrazolyl)-borate], an absorption shoulder of moderate intensity observed in the UV/vis spectrum at 23000 cm^{-1} ($\varepsilon \sim 500$ $Lmol^{-1}cm^{-1}$) has also been assigned to the $d_{xy} \rightarrow d_{x^2-y^2}$ ligand-field transition based on analysis of the corresponding MCD spectrum.[2] However, there is no reasonable explanation for the unusually high intensity of this ligand-field transition in the case of [Mo(O)Cl_3dppe], especially when compared to the broad absorption band A at 15500 cm^{-1}, which is assigned to the $d_{xy} \rightarrow d_{xz}$, d_{yz} ligand-field transition, in accordance with the literature.[2,9,39,40]

The third ligand-field transition, $d_{xy} \rightarrow d_{z^2}$, is expected at energies greater than 35000 cm^{-1} and thus is not observed in the UV/vis spectrum of [Mo(O)Cl_3dppe] because it is superimposed by more intense charge-transfer transitions.[41]

Additionally, four shoulders can be identified at 25000 cm^{-1} (band D), 30000 cm^{-1} (band E), 34000 cm^{-1} (band F), and 36000 cm^{-1} (band G) in the tail of a rising absorbance (Figure 3). They might arise from various Cl → Mo charge-transfer transitions (LMCT). In addition, the possible presence of Mo → P metal-to-ligand charge transfer (MLCT) as well as O → Mo LMCT has to be taken into account. Obviously, the UV/vis spectrum alone is not sufficient to arrive at a reliable assignment of the observed electronic transitions. Thus, low-temperature MCD spectra were recorded that provide further information with respect to the ligand-field and charge-transfer excited states of the title complex.

Low-Temperature MCD Spectra. In the low-temperature MCD spectrum of [Mo(O)Cl_3dppe], four distinct absorption features are observed between 20000 and 37000 cm^{-1} with two points of zero crossing at 27000 and 32000 cm^{-1} (Figure 4). This is different from the band pattern observed in the MCD spectra of any of the C_S-symmetric oxidomolybdenum(V) [Mo-(O)X_2L] complexes [L = hydrotris(3,5-dimethyl-1-pyrazolyl)-borate; X = O (diol, chatecholato), Cl, or S (dithiolato)] that have already been reported.[2,9,23]

The features of the MCD spectrum could successfully be modeled by six Gaussian curves (Figure 4, top). At positive magnetic field strengths, three positive bands (bands 1−3) are observed between 20000 and 25000 cm^{-1}. They are followed by two transitions with negative MCD intensities around 30000 cm^{-1} (bands 4 and 5) and another positive band centered at 34100 cm^{-1} (band 6).

There is a good correlation of the most intense MCD transition (band 1) with the UV/vis absorption band B at 20500 cm^{-1}. The presence of the additional low-intensity band C in the UV/vis absorption spectrum, which is superimposed by the more intense band B, is now confirmed by the presence of the MCD band 2 at 21100 cm^{-1}. The positions of the MCD bands 3, 4/5, and 6 roughly correspond to the observed shoulders in the UV/vis spectrum at 25000, 30000, and 34000 cm^{-1} (bands D−F).

The MCD bands 3−6 all show the same intensity in a positive−negative−negative−positive pattern and should therefore be considered as two corresponding *pseudo-A* terms, a negative *pseudo-A* term centered at 27000 cm^{-1} (bands 3 and 4), and a positive *pseudo-A* term centered at 32500 cm^{-1} (bands 5 and 6), giving rise to a so-called "double *pseudo-A* term". This implies that both the donor and acceptor orbitals derive from two pairs of nearly degenerate orbitals of appropriate symmetry and that the transition-dipole moments of the individual

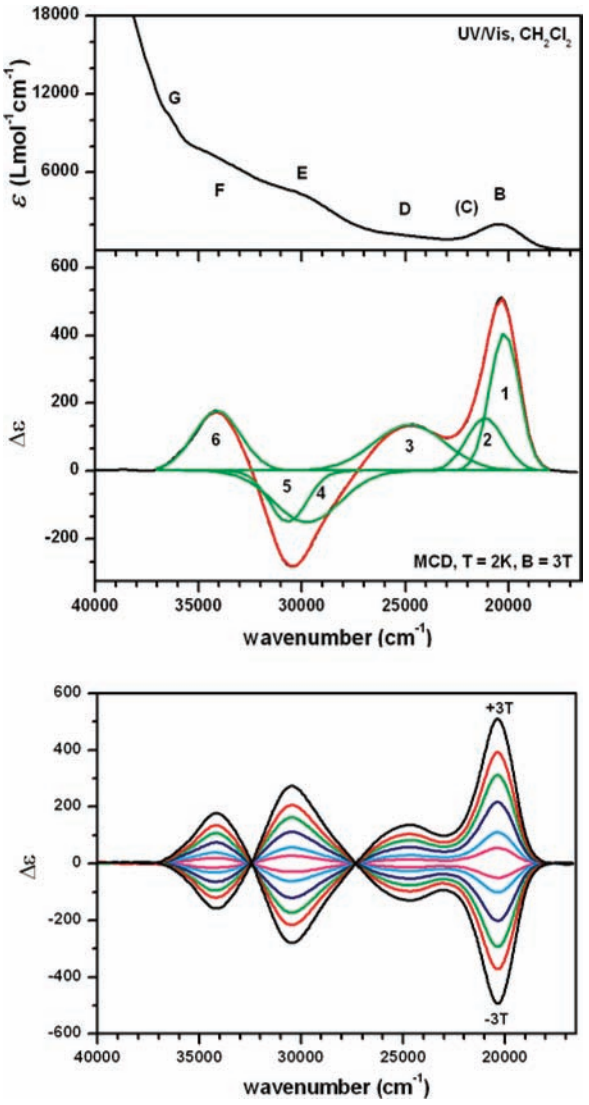

Figure 4. (Bottom) Low-temperature MCD spectra of [Mo(O)-Cl_3dppe] measured in polystyrene/CH_2Cl_2 at T = 2 K. The sample was prepared from a 1 mM solution of the title complex. The magnetic field strength was varied from B = −3 to +3 T. (Top) Gaussian curve fit of the low-temperature MCD spectrum obtained at T = 2 K and B = 3 T between 20000 and 37000 cm^{-1}. The UV/vis absorption spectrum recorded at room temperature is shown for comparison.

transitions between these orbitals each have opposite signs (vide supra). A "double *pseudo-A* term" has also been identified as the dominating spectral feature in the MCD spectra of several molybdenum(V) oxido−dithiolato complexes and was assigned to S → Mo LMCT transitions.[2,9,23]

A detailed assignment of the observed UV/vis and MCD transitions is possible based on the TDDFT calculation of the electronic transitions, as well as MO and symmetry considerations, which will also give an explanation for the positive and negative signs of the individual MCD bands.

DFT Evaluation of the MO Scheme. The MOs of [Mo(O)Cl_3dppe] obtained from an unrestricted DFT calculation do not show a large extent of spin polarization, with the only exception of the singly occupied molecular orbital (MO 117). α and β spin orbitals thus coincide in orbital numbers and orbital types, so Figure 5 only shows the relevant α spin

dx.doi.org/10.1021/ic300201t | Inorg. Chem. 2012, 51, 5748−5763

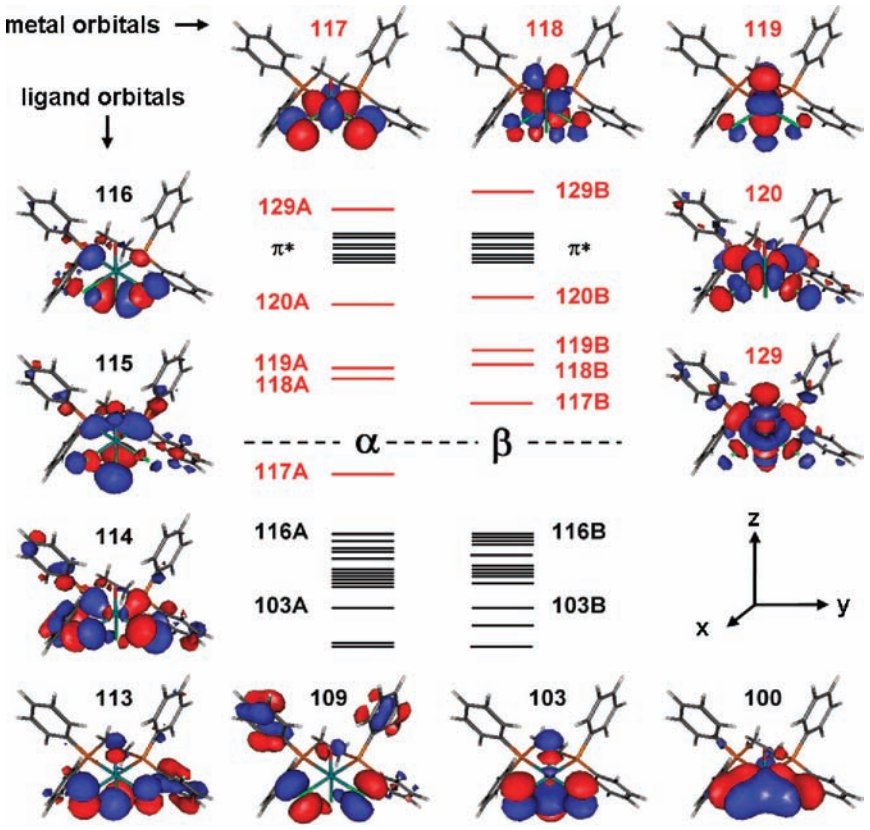

Figure 5. MOs (α spin orbitals) of [Mo(O)Cl_3dppe] as obtained from the DFT calculation (BP86/LANL2DZ).

Table 3. MOs of [Mo(O)Cl_3dppe] Obtained from the DFT Calculation (BP86/LANL2DZ)

		sym[a]	Mo	Cl_{eq}	Cl_{ax}	O	description
129	z^2	a′	d_{z^2}	$\sigma_{sym}(Cl_{eq}+P)$	p_z	p_z	σ-antibonding, unoccupied metal d orbital phenyl π^* orbitals
120	xy	a″	d_{xy}	$\sigma_2(Cl_{eq}+P)$			σ-antibonding, unoccupied metal d orbital
119	xz	a′	d_{xz}	$p_{out\text{-}of\text{-}plane}$ (s)	p_x	p_x	π-antibonding, unoccupied metal d orbital
118	yz	a″	d_{yz}	$p_{out\text{-}of\text{-}plane}$ (a)	p_y	p_y	π-antibonding, unoccupied metal d orbital
117	$x^2 - y^2$	a′	$d_{x^2-y^2}$	$p_{in\text{-}plane}$ (s)			$d_{x^2-y^2}/p_{in\text{-}plane}$, π-antibonding, singly occupied metal d orbital
116	$p_y(Cl_{ax})$	a″		"e"(Cl_{eq}+P)	p_y	(p_y)	axial chlorido p orbital (Cl_{ax})
115	$p_x(Cl_{ax})$	a′		"e"(Cl_{eq}+P)	p_x	(p_x)	axial chlorido p orbital (Cl_{ax})
114	$p_{in\text{-}plane}$(a)	a″		$p_{in\text{-}plane}$ (a)	(p_y)		in-plane ligand p orbital (Cl_{eq})
113	$p_{out\text{-}of\text{-}plane}$(s)	a′		$p_{out\text{-}of\text{-}plane}$ (s)	p_x	p_x	out-of-plane chlorido p_π orbital, p_x antibonding phenyl π orbitals
109	$p_{out\text{-}of\text{-}plane}$(a)	a″		$p_{out\text{-}of\text{-}plane}$ (a)	p_y	(p_y)	out-of-plane chlorido p_π orbital (Cl_{eq}) phenyl π orbitals
103	$p_{out\text{-}of\text{-}plane}$(s)	a′		$p_{out\text{-}of\text{-}plane}$ (s)	p_x	p_x	out-of-plane chlorido p_π orbital (Cl_{eq}), p_x binding $p(Cl_{eq}) + sp^3(P)$
100	$x^2 - y^2$	a′	$d_{x^2-y^2}$	$p_{in\text{-}plane}$(s)			$d_{x^2-y^2}/p_{in\text{-}plane}$, π-binding analogue of MO 117
95	xy	a″	d_{xy}	$\sigma_2(Cl_{eq}+P)$			d_{xy}/σ_2, σ-binding analogue of MO 120
82	z^2	a′	d_{z^2}	$\sigma_{sym}(Cl_{eq}+P)$	p_z	p_z	d_{z^2}/σ_{sym}, σ-binding analogue of MO 129

[a] C_S symmetry (mirror plane xz).

orbitals, which are also listed and described in Table 3. Compared to the qualitative ligand-field diagram shown in Figure 3 (inset), the expected energy sequence of the metal d orbitals is confirmed by DFT.

For a C_S-symmetrical complex, the mirror plane (xz) defines the molecular axes, so that the d_{xy} orbital, which is the highest (singly!) occupied molecular orbital (MO 117), has to be relabeled into $d_{x^2-y^2}$ (and vice versa). The four unoccupied metal d orbitals are d_{yz} and d_{xz} (MO 118 and MO 119), d_{xy} (MO 120, formerly $d_{x^2-y^2}$), and d_{z^2} (MO 129).

The energetically highest ligand orbitals are the p_y and p_x orbitals of the axial chlorido ligand (MO 116 and MO 115). To describe the p orbitals of the equatorial chlorido ligands, four possible linear combinations have to be considered because both the in-plane and out-of-plane p_π orbitals can be combined symmetrically (s) or antisymmetrically (a) with respect to the molecular mirror plane xz. Additionally, the bonding and

dx.doi.org/10.1021/ic300201t | Inorg. Chem. 2012, 51, 5748−5763

antibonding interactions with the corresponding metal d orbitals and the p orbitals of the axial ligands have to be taken into account. The symmetric combination of the in-plane p_π orbitals is stabilized by the metal $d_{x^2-y^2}$ orbital, resulting in a bonding and an antibonding combination (MO 100 and MO 117). In contrast, the antisymmetric in-plane p_π orbital cannot be stabilized by any of the Mo d orbitals but instead shows a large contribution of P sp^3 orbitals (MO 114).

The symmetric linear out-of-plane p_π orbital interacts with the p_x orbital of the axial chlorido ligand, again resulting in a bonding and an antibonding linear combination (MO 103 and MO 113). It also interacts with the d_{xz} orbital: MO 119 exhibits an antibonding interaction, whereas the bonding analogue is not observed among the 20 highest occupied MOs. The antisymmetric out-of-plane p_π orbital shows a large percentage of phenyl π orbitals (MO 109). It can also interact with the d_{yz} orbital: MO 118 exhibits an antibonding interaction, whereas the bonding analogue is again not observed among the 20 highest occupied MOs. The σ-bonding counterparts of the unoccupied d_{xy} and d_{z^2} metal d orbitals, in contrast, can be clearly identified in the manifold of the higher-lying occupied MOs (MO 95 and MO 82, not shown in Figure 5). Because of molecular symmetry, all MOs are either symmetric (a′) or antisymmetric (a″) with respect to the mirror plane xz. MOs that are not displayed in Figure 5 are mainly π and π^* orbitals of the dppe phenyl groups. Some of them show significant contributions of the different p_{Cl} orbitals, and the occupied dppe π orbitals are often mixed with the $p_{out\text{-}of\text{-}plane}(a)$ orbital (MO 105, MO 107, and MO 111). There are no α or β spin orbitals among the 20 highest occupied MOs, which exhibit pure phosphorus or oxido p character.

The same types of MOs have also been described for the molybdenum(V) oxido−chlorido complex $[Mo(O)Cl_2L]$ [L = hydrotris(3,5-dimethyl-1-pyrazolyl)borate],[2] with the exception of the axial p_{Cl} orbitals because no axial chlorido ligand was present in this complex. Because of this difference in coordination, the symmetric and antisymmetric equatorial out-of-plane p_π orbitals and the d_{xz} and d_{yz} orbitals are inverted in energy in the case of $[Mo(O)Cl_3dppe]$ compared to $[Mo(O)Cl_2L]$ [L = hydrotris(3,5-dimethyl-1-pyrazolyl)borate].[2] The same also applies for the corresponding oxidomolybdenum(V) dithiolate complexes $[Mo(O)S_2L]$.[2,9,23]

TDDFT Calculation of the Electronic Transitions and Assignment of the UV/Vis Spectrum. The electronic transitions of $[Mo(O)Cl_3dppe]$ were calculated by TDDFT. The results are shown in Figure 6 and Table 4, respectively. The most intense electronic transitions in the calculated UV/vis spectrum are various LMCT transitions from different p_{Cl} orbitals into the d_{xy} orbital at energies of around 35000 cm^{-1}, probably corresponding to the weak shoulder at 36000 cm^{-1} (band G) in the experimental UV/vis spectrum. An additional shoulder is calculated at 26000 cm^{-1}, which might correspond to the observed shoulder at 25000 cm^{-1} (band D) in the experimental UV/vis spectrum.

The energies of the $d_{x^2-y^2} \rightarrow d_{xz}$, d_{yz} ligand-field transitions, which are observed at 15500 cm^{-1} in the experimental UV/vis absorption spectrum, appear too low in the calculated spectrum (11900 and 13600 cm^{-1}). In contrast, the calculated $d_{x^2-y^2} \rightarrow d_{xy}$ transition is found at 21100 cm^{-1}. This perfectly matches the energy of the UV/vis absorption band C, which corresponds to the MCD band 2 at 21100 cm^{-1}. The most intense transition in the spectral region around 20000 cm^{-1} of the calculated spectrum is the $p_{in\text{-}plane}(a) \rightarrow d_{x^2-y^2}$ LMCT transition

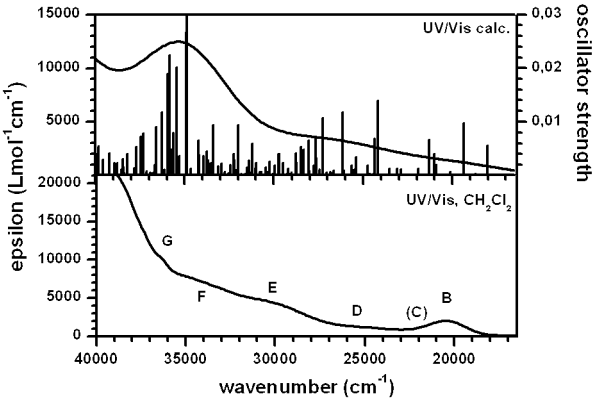

Figure 6. Experimental and calculated UV/vis spectra of $[Mo(O)Cl_3dppe]$ shown for comparison. The experimental UV/vis spectrum was measured in CH_2Cl_2. The calculated UV/vis spectrum was computed by TDDFT (B3LYP/LANL2DZ).

at 19500 cm^{-1}, which is in good agreement with the experimentally observed UV/vis absorption band B at 20500 cm^{-1} and the MCD band 1, respectively. The calculated energy of the $d_{x^2-y^2} \rightarrow d_{z^2}$ ligand-field transition is 33600 cm^{-1}. This is in good accordance with the predicted energy of ∼35000 cm^{-1} for the experimental energy.[41]

The TDDFT calculations also provide information with respect to LMCT transitions to the unoccupied metal d orbitals. Theoretically, such transitions can either occur within the α or β spin orbitals, but because no spin polarization between these two sides has been observed in the calculation of the MOs (vide supra), no splitting is expected between the corresponding LMCT transitions in the manifolds of spin-up and spin-down orbitals.

The LMCT transitions from the p orbitals of the axial chlorido ligand into the d_{yz} and d_{xz} orbitals are predicted between 21000 and 28000 cm^{-1}. The most intense of these transitions in the calculated UV/vis spectrum, $p_x \rightarrow d_{yz}$, is found at 24300 cm^{-1}, which might correspond to the experimentally observed absorption feature at 25000 cm^{-1} (band D) and thus to band 3 in the MCD spectrum.

LMCT transitions originating from the symmetric out-of-plane p_π orbital of the equatorial chlorido ligands (MO 113) are found at 26200 and 28600 cm^{-1}, ($p_{out\text{-}of\text{-}plane}(s) \rightarrow d_{yz}$, d_{xz}) and might correspond to the observed shoulders at 25000 cm^{-1} (band D) and 30000 cm^{-1} (band E) in the experimental UV/vis spectrum and thus to bands 3 and 4, i.e., the negative *pseudo-A* term, in the MCD spectrum. The corresponding $p_{out\text{-}of\text{-}plane}(a) \rightarrow d_{yz}$, d_{xz} transitions, in contrast, only appear with very low intensities in the calculated UV/vis spectrum.

A possible assignment of the observed shoulder at 36000 cm^{-1} (band G) in the experimental UV/vis absorption spectrum might be the $p_{in\text{-}plane}(a) \rightarrow d_{xy}$ transition (MO 114 → MO 120), which shows a very high intensity in the calculated UV/vis spectrum at 35000 cm^{-1}.

Considering the overall spectral shape, a clear-cut correlation between the experimental and theoretical UV/vis spectra is not possible. Although some trends considering the types of electronic transitions (d → d, LMCT) can be obtained for particular spectral regions, a definite assignment of the observed UV/vis transitions (which can also be transferred to the assignment of the MCD spectrum) is not possible based on the TDDFT calculation alone. Additionally, this type of calculation

dx.doi.org/10.1021/ic300201t | Inorg. Chem. 2012, 51, 5748−5763

Table 4. Electronic Transitions of [Mo(O)Cl$_3$dppe] Calculated by TDDFT (B3LYP/LANL2DZ) (Only d → d Ligand-Field and Charge-Transfer Transitions with Oscillator Strengths >0.0020 Are Listed)

energy (cm^{-1})	oscillator strength	description	assignment	leading MO contribution
11900	0.0007	$x^2-y^2 \rightarrow yz$	d → d	117A → 118A
13600	0.0003	$x^2-y^2 \rightarrow xz$	d → d	117A → 119A
18200	0.0056	$p_y \rightarrow x^2-y^2$	L_{ax}MCT	116B → 117B
19500	0.0098	$p_{in\text{-}plane}(a) \rightarrow x^2-y^2$	L_{eq}MCT	114B → 117B
21100	0.0020	$p_y \rightarrow yz$	L_{ax}MCT	116B → 118B
21100	0.0040	$x^2-y^2 \rightarrow xy$	d → d	117A → 120A
21400	0.0067	$p_x \rightarrow yz$	L_{ax}MCT	115A → 118A
24300	0.0139	$p_x \rightarrow yz$	L_{ax}MCT	115A → 118A
24500	0.0069	$p_x/p_y \rightarrow yz$	L_{ax}MCT	115/116B → 118B
26200	0.0118	$p_{out\text{-}of\text{-}plane}(s) \rightarrow yz$	L_{eq}MCT	113B → 118B
27400	0.0107	$p_x \rightarrow xz$	L_{ax}MCT	115B → 119B
27700	0.0032	$p_{out\text{-}of\text{-}plane}(s,a) \rightarrow xy, yz$	L_{eq}MCT	103/105 → 117/118
28200	0.0066	phenyl $\pi \rightarrow xz$	LMCT	104A → 119A
28400	0.0049	phenyl π $[p_{out\text{-}of\text{-}plane}(a)] \rightarrow yz$	L_{eq}MCT	106/112A → 118A
28600	0.0054	$p_{out\text{-}of\text{-}plane}(s) \rightarrow xz$	L_{eq}MCT	113B → 119B
28800	0.0023	$p_{out\text{-}of\text{-}plane}(a)$, phenyl $\pi \rightarrow yz$	L_{eq}MCT	110A → 118A
28900	0.0042	phenyl π $[p_{in\text{-}plane}(a)] \rightarrow xz$	L_{eq}MCT	112A → 119A
29600	0.0024	phenyl π $[p_{out\text{-}of\text{-}plane}(a)] \rightarrow xz$	L_{eq}MCT	105B → 119B
30300	0.0024	$p_{out\text{-}of\text{-}plane}(a)$ (phenyl π) → yz	LMCT	109/110B → 118B
31100	0.0024	$p_{out\text{-}of\text{-}plane}(a)$ (phenyl π) → xz	LMCT	109/110 → 118/119
31300	0.0059	$p_{in\text{-}plane}(s) \rightarrow x^2-y^2$	L_{eq}MCT	100B → 117B
31500	0.0028	$p_{out\text{-}of\text{-}plane}(a) \rightarrow yz$	L_{eq}MCT	107B → 118B
32100	0.0094	$p_x \rightarrow xy$	L_{ax}MCT	115A → 120A
32300	0.0029	$p_{out\text{-}of\text{-}plane}(s,a) \rightarrow yz, xz$	L_{eq}MCT	103/107 → 118/119
32300	0.0040	$p_{out\text{-}of\text{-}plane}(a)$, phenyl $\pi \rightarrow xz$	LMCT	109/110B → 119B
32500	0.0020	$p_{out\text{-}of\text{-}plane}(a) \rightarrow yz, xz$	L_{eq}MCT	107/111B → 118/119B
33000	0.0022	$p_{in\text{-}plane}(a)$, $p_y \rightarrow xy$	L_{eq}/L_{ax}MCT	114/116A → 120A
33400	0.0094	phenyl π $[p_{out\text{-}of\text{-}plane}(s)] \rightarrow xz$	L_{eq}MCT	108B → 119B
33400	0.0034	$p_{in\text{-}plane}(s)$, $p_{out\text{-}of\text{-}plane}(s) \rightarrow yz$	L_{eq}MCT	102/103B → 119B
33600	0.0023	phenyl π $[p_{out\text{-}of\text{-}plane}(a)] \rightarrow xz$	L_{eq}MCT	108B → 119B
		$x^2-y^2 \rightarrow z^2$	d → d	117A → 129A
33700	0.0028	$p_{in\text{-}plane}(s)/x^2-y^2 \rightarrow yz$	L_{eq}MCT	102B → 118B
33800	0.0045	phenyl $\pi \rightarrow xz$, $p_{out\text{-}of\text{-}plane}(s) \rightarrow xy$	L_{eq}MCT	106B → 119B, 113A → 120A
34000	0.0038	$p_{out\text{-}of\text{-}plane}(s) \rightarrow xy$	L_{eq}MCT	113A → 120A
34300	0.0065	$p_{in\text{-}plane}(a)$, $p_y \rightarrow xy$	L_{eq}/L_{ax}MCT	114/116A → 120A
34900	0.1067	$p_x \rightarrow xy$	L_{ax}MCT	115A → 120A
35000	0.0267	$p_{in\text{-}plane}(a) \rightarrow xy$	L_{eq}MCT	114A → 120A
35400	0.0029	$p_{in\text{-}plane}(s)$, $p_{out\text{-}of\text{-}plane}(s) \rightarrow xz$	L_{eq}MCT	102/103 → 119
35500, 35700	0.0201, 0.0080	ligand $\sigma \rightarrow x^2-y^2$		96/97B → 117B
35800	0.0048	$p_{in\text{-}plane}(s)$, $p_{out\text{-}of\text{-}plane}(s) \rightarrow xy$	L_{eq}MCT	102/103 → 120
35900	0.0225	$p_{out\text{-}of\text{-}plane}(s) \rightarrow xy$	L_{eq}MCT	113A → 120A

gives no explanation of the positive and negative signs of the individual MCD transitions. Therefore, an assignment of the electronic transitions on the basis of MO considerations is presented in the following section.

Assignment of the Electronic Transitions Based on the MO Scheme and Symmetry Considerations. In addition to the results of TDDFT, also the MO scheme of [Mo(O)Cl$_3$dppe] (Figure 5) suggests that LMCT transitions from p_{Cl} orbitals to the singly occupied $d_{x^2-y^2}$ orbital and the $d_{x^2-y^2} \rightarrow d_{xy}$ ligand-field transition are the lowest-energy transitions and should appear in the spectral region between 19000 and 25000 cm^{-1} according to the literature.[2,9,23] The actual assignment of the MCD bands 1 and 2, which correspond to the UV/vis absorption bands B and C, is supported by resonance Raman measurements (Figure 7).

The resonance Raman spectra obtained at the excitation energies of 19500 and 22000 cm^{-1} reveal that the symmetric Mo−Cl_{eq} stretching vibration at 332 cm^{-1} and the Mo−P stretch at 523 cm^{-1}, which are both in-plane vibrations, are very strongly enhanced compared to the "off-resonance" FT-Raman spectrum (Figure 2, top). In contrast, the Mo=O stretch (perpendicular to the *xy* plane) at 943 cm^{-1} is not enhanced in these resonance Raman spectra. Its relative intensity is even reduced compared to the "off-resonance" FT-Raman spectrum (Figure 2, top). This clearly indicates that only in-plane metal and ligand orbitals are involved in electronic transitions within this spectral region. LMCT from the axial chlorido ligands to metal d orbitals is therefore ruled out for the assignment of the MCD bands 1 and 2 and the UV/vis bands B and C, respectively.

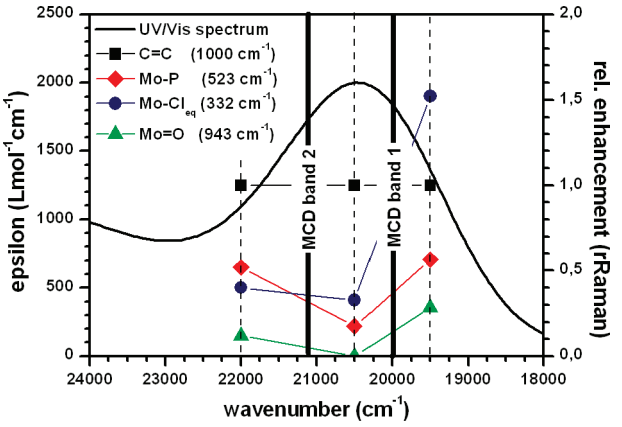

Figure 7. UV/vis absorption spectrum of [Mo(O)Cl$_3$dppe] between 18000 and 24000 cm^{-1} and resonance Raman excitation profile of the characteristic metal−ligand vibrations. The relative enhancement of the individual metal−ligand vibrations in the resonance Raman spectra is referred to the dppe phenyl C=C ring-breathing vibration at 1000 cm^{-1}. The bold lines denote the positions of the MCD bands 1 and 2. The dashed lines represent the excitation energies of the resonance Raman spectra.

Using the excitation energy of 19500 cm^{-1}, especially the Mo−Cl_{eq} vibration is very strongly enhanced in the resonance Raman spectrum. It receives 150% of the intensity of the symmetric dppe phenyl C=C ring-breathing vibration at 1000 cm^{-1} compared to only 40% in the "off-resonance" FT-Raman spectrum (Figure 2, top). In accordance with the TDDFT calculation (Table 4), the MCD band 1 and the corresponding UV/vis

dx.doi.org/10.1021/ic300201t | Inorg. Chem. 2012, 51, 5748−5763

absorption band B are therefore assigned to the in-plane LMCT transition from the antisymmetric in-plane Cl p_π orbital $p_{in\text{-}plane}(a)$ to the singly occupied $d_{x^2-y^2}$ orbital (MO 114 → MO 117).

The MCD band 2 at 21100 cm^{-1} corresponding to the UV/vis band C hidden beneath the more intense charge-transfer band B is then assigned to the $d_{x^2-y^2} \rightarrow d_{xy}$ ligand-field transition (MO 117 → MO 120). The d_{xy} orbital is antibonding with respect to the equatorial σ_{Cl} and σ_P ligand orbitals (σ_2; Figure 5), which explains the moderate enhancement of the Mo−Cl_{eq} and Mo−P stretches in the resonance Raman spectrum at this energy. The higher absorption intensity of this UV/vis band compared to the $d_{x^2-y^2} \rightarrow d_{xz}$, d_{yz} ligand-field transition (band A) is supported by the results of TDDFT (Table 4).

The MCD bands 3−6 all exhibit the same intensities in a positive−negative−negative−positive pattern of two corresponding *pseudo-A* terms. This implies that both the donor and acceptor orbitals derive from two pairs of (almost) degenerate orbitals of appropriate symmetry and that the transition-dipole moments of the individual transitions between these orbitals each have opposite signs (vide supra). Three pairs of almost or formerly degenerate orbitals can be identified in the MO scheme (Figure 5) of [Mo(O)Cl_3dppe], which are (i) the p_y and p_x orbitals of the axial chlorido ligand trans to the oxido group, (ii) the symmetric and antisymmetric out-of-plane p_π orbitals of the equatorial chlorido ligands $p_{out\text{-}of\text{-}plane}(s,a)$, and (iii) the metal d_{yz} and d_{xz} orbitals. Note that all three pairs of orbitals show a change of symmetry with respect to the molecular mirror plane *xz*.

Although the $p_x \rightarrow d_{yz}$, d_{xz} transitions are indeed predicted by TDDFT as possible assignments for the MCD bands 3 and 4 from their calculated energies, this possibility is not considered for the following reason: The $p_x \rightarrow d_{xz}$ and the $p_y \rightarrow d_{yz}$ transitions are both *z*-polarized, while the transition densities of the $p_x \rightarrow d_{yz}$ and the $p_y \rightarrow d_{xz}$ transitions are zero. The p_x, $p_y \rightarrow d_{yz}$, d_{xz} transitions are thus expected to result only in two equally signed MCD bands but cannot give rise to a "double *pseudo-A* term" and are therefore ruled out for the assignment of the MCD bands 3−6.

Thus, the only possibility is the assignment of the "double *pseudo-A* term" to the Mo → Cl LMCT from the equatorial out-of-plane p_π orbitals, $p_{out\text{-}of\text{-}plane}(s,a)$, to the d_{yz} and d_{xz} orbitals. The $p_{out\text{-}of\text{-}plane}(s) \rightarrow d_{yz}$, d_{xz} transition was already predicted by the TDDFT calculation as another possibility for the assignment of the MCD bands 3 and 4 (negative *pseudo-A* term), while the $p_{out\text{-}of\text{-}plane}(a) \rightarrow d_{yz}$, d_{xz} transitions were only found with relatively low intensities in the calculated UV/vis spectrum. According to the MO scheme (Figure 5), however, they should appear at higher energies than bands 3 and 4 and might therefore be assigned to the positive *pseudo-A* term at 32500 cm^{-1} (bands 5 and 6).

As was already mentioned, the UV/vis absorption band G might be assigned to the $p_{in\text{-}plane}(a) \rightarrow d_{xy}$ transition. From the MO scheme and computation of the electronic transitions by TDDFT, no evidence is given for Mo → P MLCT or O → Mo LMCT transitions.

The complete assignment of the individual electronic transitions is summarized in Table 5.

Theory of the MCD *C*-Term Intensities for Multideterminant Excited Doublet States. To verify the assignment of the observed "double *pseudo-A* term", a general procedure for the determination of the MCD *C*-term intensities is applied.[1] The Mo → Cl LMCT transitions from the symmetric and antisymmetric out-of-plane p_π orbitals to the d_{xz} and d_{yz} are from doubly occupied MOs (*i* and *j*) to unoccupied MOs (*a* and *b*) and thus clearly correspond to type III electronic transitions (vide supra). In this case, the multideterminant character of the excited states has to be taken into account.[20] The resulting expressions for the MCD *C*-term intensity in terms of states are then converted into expressions in terms of one-electron orbitals. Finally, the signs of the MCD bands are determined from the transition densities of the individual transitions considering overlap of the involved donor and acceptor MOs.

Table 5. Assignment of the Electronic Transitions (given in cm^{-1}) of [Mo(O)Cl_3dppe])

UV/vis	MCD	TDDFT	assignment	
(A) 15500		11900, 13600	$x^2-y^2 \rightarrow -yz, xz$	d → d
(B) 20500	(1) 20000 (+)	19500	$p_{in\text{-}plane}(a) \rightarrow x^2-y^2$	L_{eq}MCT
(C)	(2) 21100 (+)	21100	$x^2-y^2 \rightarrow xy$	d → d
(D) 25000	(3) 24800 (+)	26200	$p_{out\text{-}of\text{-}plane}(s) \rightarrow yz$	L_{eq}MCT
(E) 30000	(4) 29600 (−)	28600	$p_{out\text{-}of\text{-}plane}(s) \rightarrow xz$	L_{eq}MCT
	(5) 30600 (−)	(28800, 30300)[a]	$p_{out\text{-}of\text{-}plane}(a) \rightarrow yz$	
(F) 34000	(6) 34100 (+)	(31100, 33600)[a]	$p_{out\text{-}of\text{-}plane}(a) \rightarrow xz$	L_{eq}MCT
(G) 36000		35000	$p_{in\text{-}plane}(a) \rightarrow xy$	L_{eq}MCT

[a]Very low intensity in the calculated UV/vis spectrum (Figure 6 and Table 4).

In the case of spin-allowed type III electronic transitions from the $S = {}^1/_2$ ground state, all excited doublet states split into sing-doublet and trip-doublet states (Scheme 2). In the case of an $i \rightarrow a$ transition, the sing-doublet $M_S = +{}^1/_2$ and $-{}^1/_2$ states correspond to

$$|C_i^a + 1/2\rangle = \frac{1}{\sqrt{2}}(|\psi_1^+\psi_1^-...\psi_i^+\psi_a^-...\psi_n^+\psi_n^-\psi_0^+| + |\psi_1^+\psi_1^-...\psi_a^+\psi_i^-...\psi_n^+\psi_n^-\psi_0^+|)$$

and

$$|C_i^a - 1/2\rangle = \frac{1}{\sqrt{2}}(|\psi_1^+\psi_1^-...\psi_i^+\psi_a^-...\psi_n^+\psi_n^-\psi_0^-| + |\psi_1^+\psi_1^-...\psi_a^+\psi_i^-...\psi_n^+\psi_n^-\psi_0^-|)$$

whereas the trip-doublet $M_S = +{}^1/_2$ and $-{}^1/_2$ excited doublet states correspond to

$$|D_i^a + 1/2\rangle = \frac{1}{\sqrt{6}}(|\psi_1^+\psi_1^-...\psi_i^+\psi_a^-...\psi_n^+\psi_n^-\psi_0^+| - |\psi_1^+\psi_1^-...\psi_a^+\psi_i^-...\psi_n^+\psi_n^-\psi_0^+| + 2|\psi_1^+\psi_1^-...\psi_i^+\psi_0^-...\psi_n^+\psi_n^-\psi_a^+|)$$

and

$$|D_i^a - 1/2\rangle = \frac{1}{\sqrt{6}}(|\psi_1^+\psi_1^-...\psi_a^+\psi_i^-...\psi_n^+\psi_n^-\psi_0^-| - |\psi_1^+\psi_1^-...\psi_i^+\psi_a^-...\psi_n^+\psi_n^-\psi_0^-| + 2|\psi_1^+\psi_1^-...\psi_0^+\psi_i^-...\psi_n^+\psi_n^-\psi_a^-|)$$

dx.doi.org/10.1021/ic300201t | *Inorg. Chem.* 2012, 51, 5748−5763

In analogy to the "luminescent states" of copper, cobalt, and vanadium porphyrin complexes considered by Ake and Gouterman, we also assume that the sing-doublet excited states are higher in energy than the trip-doublet excited states; i.e., $E(C_i^a) > E(D_i^a)$.[42]

The transition from the electronic ground state to a sing-doublet excited state has electric-dipole intensity. Assuming the ground-state configuration to be $|\psi_i^+\psi_i^-\psi_0^+\rangle$, the transition-dipole moment of a sing-doublet excitation is given by

$$\begin{aligned}\langle \psi_i^+\psi_i^-\psi_0^+|\underline{\mu}|C_i^a + 1/2\rangle &= \frac{1}{\sqrt{2}}\{\langle \psi_i^+\psi_i^-\psi_0^+|\underline{\mu}|\psi_i^+\psi_a^-\psi_0^+\rangle \\ &\quad + \langle \psi_i^+\psi_i^-\psi_0^+|\underline{\mu}|\psi_a^+\psi_i^-\psi_0^+\rangle\} \\ &= \frac{1}{\sqrt{2}}\{\langle \psi_i^-|\underline{\mu}|\psi_a^-\rangle + \langle \psi_i^+|\underline{\mu}|\psi_a^+\rangle\} \\ &= \sqrt{2}\langle \psi_i|\underline{\mu}|\psi_a\rangle \neq 0\end{aligned}$$

However, because of the form of the generalized spin–orbit coupling operator $\bar{L}_z$, two sing-doublet excited states C_i^a $(i \rightarrow a)$ and $C_i^b(i \rightarrow b)$ do *not* interact via spin–orbit coupling, even if the l_z matrix element between ψ_a and ψ_b is nonzero:

$$\begin{aligned}&\langle C_i^a + 1/2|\sum_i l_z(i)\, s_z(i)|C_i^b + 1/2\rangle \\ &= \frac{1}{2}\{\langle \psi_a^-|l_z s_z|\psi_b^-\rangle + \langle \psi_a^+|l_z s_z|\psi_b^+\rangle\} \\ &= \frac{1}{2}\left\{-\frac{1}{2}\langle \psi_a|l_z|\psi_b\rangle + \frac{1}{2}\langle \psi_a|l_z|\psi_b\rangle\right\} = 0\end{aligned}$$

These transitions therefore do *not* contribute to the MCD *C*-term intensity in zeroth order.

The trip-doublet excited states D_i^a $(i \rightarrow a)$ and D_i^b $(i \rightarrow b)$, in contrast, do interact via spin–orbit coupling,

$$\langle D_i^a + 1/2|\sum_i l_z(i)\, s_z(i)|D_i^b + 1/2\rangle = 2/3\langle \psi_a|l_z|\psi_b\rangle \neq 0$$

and thus theoretically give rise to the MCD *C*-term intensity. Moreover, the following mixed sing-doublet/trip-doublet spin–orbit coupling terms are also nonzero:

$$\begin{aligned}&\langle D_i^a + 1/2|\sum_i l_z(i)\, s_z(i)|C_i^b + 1/2 \\ &= \langle C_i^a + 1/2|\sum_i l_z(i)\, s_z(i)|D_i^b + 1/2\rangle \\ &= -\frac{1}{\sqrt{12}}\langle \psi_a|l_z|\psi_b\rangle \neq 0\end{aligned}$$

However, the transition-dipole moments between the ground state and the trip-doublet excited states, e.g., $\langle \psi_i^+\psi_i^-\psi_0^+|\underline{\mu}|D_i^a + {}^1/_2\rangle$, are zero, so that the trip-doublet excited states are, in fact, not accessible from the ground state by electronic dipole transitions, and spin–orbit coupling between the sing-doublet and trip-doublet states will not provide a mechanism for the *C*-term intensity.

Nevertheless, configuration interaction (CI) between the sing-doublet and trip-doublet excited states provides a mechanism that gives rise to nonzero MCD *C*-term intensity for type III electronic transitions, as will be shown now. From CI, new states result as

$$A_+ = (\sin\theta)C_i^a + (\cos\theta)D_i^a \quad (1)$$

$$A_- = (\cos\theta)C_i^a - (\sin\theta)D_i^a \quad (2)$$

$$B_+ = (\sin\theta)C_i^b + (\cos\theta)D_i^b \quad (3)$$

$$B_- = (\cos\theta)C_i^b - (\sin\theta)D_i^b \quad (4)$$

Note that θ is small if the sing-doublet excited states are much higher in energy than the trip-doublet states, i.e., $E(C_i^{a,b}) \gg E(D_i^{a,b})$, and the CI matrix element is small (see below).[42] In this case, the main contributions to the A_+ and B_+ excited states are the trip-doublet states, while the A_- and B_- excited states are dominated by the sing-doublet contributions. The mixing coefficient $\sin\theta$ is given by

$$\sin\theta = \frac{\langle C_i^a|\sum_{i<j}\frac{e^2}{r_{ij}}|D_i^a\rangle}{\Delta E(C_i^a - D_i^a)}$$

$$\text{with } \langle C_i^a|\sum_{i<j}\frac{e^2}{r_{12}}|D_i^a\rangle = \frac{\sqrt{3}}{2}(K_{ao} - K_{io})^{42}$$

which is positive if $K_{ao} > K_{io}$ (K_{ao}, K_{io} = exchange integrals).

Both *A* states interact through spin–orbit coupling with both *B* states:

$$\begin{aligned}&\langle A_+|\sum_i l_z(i)\, s_z(i)|B_+\rangle \\ &= \sin\theta\cos\theta\langle C_i^a|\sum_i l_z(i)\, s_z(i)|D_i^b\rangle + \cos\theta\sin\theta\langle D_i^a| \\ &\times \sum_i l_z(i)\, s_z(i)|C_i^b\rangle + \cos^2\theta\langle D_i^a|\sum_i l_z(i)\, s_z(i)|D_i^b\rangle \\ &= 2\sin\theta\cos\theta\left(-\frac{1}{\sqrt{12}}\right)\langle \psi_a|l_z|\psi_b\rangle + \cos^2\theta\left(\frac{2}{3}\right)\langle \psi_a|l_z|\psi_b\rangle \\ &= \left(-\frac{1}{\sqrt{3}}\right)\langle \psi_a|l_z|\psi_b\rangle\sin\theta\cos\theta + \left(\frac{2}{3}\right)\langle \psi_a|l_z|\psi_b\rangle\cos^2\theta \\ &= \left(-\frac{1}{\sqrt{3}}\sin\theta\cos\theta + \frac{2}{3}\cos^2\theta\right)\langle \psi_a|l_z|\psi_b\rangle\end{aligned}$$

$$\begin{aligned}&\langle A_+|\sum_i l_z(i)\, s_z(i)|B_-\rangle \\ &= -\sin^2\theta\langle C_i^a|\sum_i l_z(i)\, s_z(i)|D_i^b\rangle + \cos^2\theta\langle D_i^a| \\ &\quad \times \sum_i l_z(i)\, s_z(i)|C_i^b\rangle - \cos\theta\sin\theta\langle D_i^a|\sum_i l_z(i)\, s_z(i)|D_i^b\rangle \\ &= (\cos^2\theta - \sin^2\theta)\left(-\frac{1}{\sqrt{12}}\right)\langle \psi_a|l_z|\psi_b\rangle \\ &\quad - \sin\theta\cos\theta\left(\frac{2}{3}\right)\langle \psi_a|l_z|\psi_b\rangle \\ &= \left(-\frac{1}{\sqrt{12}}(\cos^2\theta - \sin^2\theta) - \frac{2}{3}\sin\theta\cos\theta\right)\langle \psi_a|l_z|\psi_b\rangle\end{aligned}$$

dx.doi.org/10.1021/ic300201t | Inorg. Chem. 2012, 51, 5748–5763

$$\begin{aligned}
&\langle A_|\sum_i l_z(i)\, s_z(i)|B_+\rangle \\
&= \cos^2\theta\langle C_i^a|\sum_i l_z(i)\, s_z(i)|D_i^b\rangle - \sin\theta\cos\theta\langle D_i^a| \\
&\quad\times\sum_i l_z(i)\, s_z(i)|D_i^b\rangle - \sin^2\theta\langle D_i^a|\sum_i l_z(i)\, s_z(i)|C_i^b\rangle \\
&= (\cos^2\theta - \sin^2\theta)\left(-\frac{1}{\sqrt{12}}\right)\langle\psi_a|l_z|\psi_b\rangle \\
&\quad - \sin\theta\cos\theta\left(\frac{2}{3}\right)\langle\psi_a|l_z|\psi_b\rangle \\
&= \left(-\frac{1}{\sqrt{12}}(\cos^2\theta - \sin^2\theta) - \frac{2}{3}\sin\theta\cos\theta\right)\langle\psi_a|l_z|\psi_b\rangle
\end{aligned}$$

and

$$\begin{aligned}
&\langle A_|\sum_i l_z(i)\, s_z(i)|B_\rangle \\
&= -\sin\theta\cos\theta\langle C_i^a|\sum_i l_z(i)\, s_z(i)|D_i^b\rangle \\
&\quad - \cos\theta\sin\theta\langle D_i^a|\sum_i l_z(i)\, s_z(i)|C_i^b\rangle \\
&\quad + \sin^2\theta\langle D_i^a|\sum_i l_z(i)\, s_z(i)|D_i^b\rangle \\
&= -2\sin\theta\cos\theta\left(-\frac{1}{\sqrt{12}}\right)\langle\psi_a|l_z|\psi_b\rangle + \sin^2\theta\left(\frac{2}{3}\right)\langle\psi_a|l_z|\psi_b\rangle \\
&= \left(\frac{1}{\sqrt{3}}\right)\langle\psi_a|l_z|\psi_b\rangle\sin\theta\cos\theta + \left(\frac{2}{3}\right)\langle\psi_a|l_z|\psi_b\rangle\sin^2\theta \\
&= \left(\frac{1}{\sqrt{3}}\sin\theta\cos\theta + \frac{2}{3}\sin^2\theta\right)\langle\psi_a|l_z|\psi_b\rangle
\end{aligned}$$

Furthermore, the individual transition-dipole matrix elements from the ground state $|A\rangle$ are given by

$$\begin{aligned}
\langle A|\mu|A_+\rangle &= \sin\theta\langle A|\mu|C_i^a\rangle + \cos 00\,\theta\langle A|\mu|D_i^a\rangle \\
&= \sin\theta\langle A|\mu|C_i^a\rangle \\
&= \sqrt{2}\,\sin\theta\langle\psi_i|\mu|\psi_a\rangle
\end{aligned}$$

$$\begin{aligned}
\langle A|\mu|A_\rangle &= \cos\theta\langle A|\mu|C_i^a\rangle - \sin\theta\langle A|\mu|D_i^a\rangle \\
&= \cos\theta\langle A|\mu|C_i^a\rangle \\
&= \sqrt{2}\,\cos\theta\langle\psi_i|\mu|\psi_a\rangle
\end{aligned}$$

$$\begin{aligned}
\langle A|\mu|B_+\rangle &= \sin\theta\langle A|\mu|C_i^b\rangle + \cos\theta\langle A|\mu|D_i^b\rangle \\
&= \sin\theta\langle A|\mu|C_i^b\rangle \\
&= \sqrt{2}\,\sin\theta\langle\psi_i|\mu|\psi_b\rangle
\end{aligned}$$

and

$$\begin{aligned}
\langle A|\mu|B_\rangle &= \cos\theta\langle A|\mu|C_i^b\rangle - \sin\theta\langle A|\mu|D_i^b\rangle \\
&= \cos\theta\langle A|\mu|C_i^b\rangle \\
&= \sqrt{2}\,\cos\theta\langle\psi_i|\mu|\psi_b\rangle
\end{aligned}$$

On the basis of the general expressions of the MCD C-term intensity given above, the C-term intensity of an xy-polarized transition $A \rightarrow J$, K ("J–K coupling") results as

$$\begin{aligned}
\frac{\Delta\varepsilon}{E} &\sim -\sum_{K\neq A,J}\frac{\bar{L}_z^{KJ}}{\Delta_{KJ}}(\vec{D}_x^{AK}\vec{D}_y^{AJ} - \vec{D}_y^{AK}\vec{D}_x^{AJ}) \\
&= -\sum_{K\neq A,J}\frac{\langle K|\bar{L}_z|J\rangle}{\Delta_{KJ}}\{\langle A|\mu_x|K\rangle\langle A|\mu_y|J\rangle - \langle A|\mu_y|K\rangle\langle A|\mu_x|J\rangle\}
\end{aligned}$$

For each individual electronic transition $A \rightarrow J$, the two different paths arising from the two possible coupling states $K = A_+/A\_$ or $B_+/B\_$ have to be summed up. Note that in the following the spin–orbit coupling matrix elements $\langle\psi_a|l_z|\psi_b\rangle$ and $\langle\psi_b|l_z|\psi_a\rangle$ are given in the short notation l_z^{ab} and l_z^{ba}, respectively. The transition-dipole matrix elements are also given in the short notation:

$$(d_x^{ib}d_y^{ia} - d_y^{ib}d_x^{ia}) = (\langle\psi_i|\mu_x|\psi_b\rangle\langle\psi_i|\mu_y|\psi_a\rangle - \langle\psi_i|\mu_y|\psi_b\rangle\langle\psi_i|\mu_x|\psi_a\rangle)$$

Moreover, contributions containing $\sin\theta$ to the power of two and three will be neglected in the final expressions as $\theta \approx 0$. The results for the four transitions then are

$$A \rightarrow J = A_+; \quad K = B_+,\ B\_$$

$$\begin{aligned}
\frac{\Delta\varepsilon}{E} &\sim -\frac{\bar{L}_z^{B_+A_+}}{\Delta_{B_+A_+}}(\vec{D}_x^{AB_+}\vec{D}_y^{AA_+} - \vec{D}_y^{AB_+}\vec{D}_x^{AA_+}) \\
&\quad - \frac{\bar{L}_z^{B_A_+}}{\Delta_{B_A_+}}(\vec{D}_x^{AB_}\vec{D}_y^{AA_+} - \vec{D}_y^{AB_}\vec{D}_x^{AA_+})
\end{aligned}$$

$$\begin{aligned}
\frac{\Delta\varepsilon}{E} &\sim -\frac{1}{\Delta_{B_+A_+}}\left(-\frac{1}{\sqrt{3}}\sin\theta\cos\theta + \frac{2}{3}\cos^2\theta\right) \\
&\quad\times \mathrm{Im}(l_z^{ba})\sin^2\theta(d_x^{ib}d_y^{ia} - d_y^{ib}d_x^{ia}) - \frac{1}{\Delta_{B_A_+}} \\
&\quad\times\left(-\frac{1}{\sqrt{12}}(\cos^2\theta - \sin^2\theta) - \frac{2}{3}\sin\theta\cos\theta\right) \\
&\quad\times \mathrm{Im}(l_z^{ba})\sin\theta\cos\theta(d_x^{ib}d_y^{ia} - d_y^{ib}d_x^{ia}) \\
&\cong 0 + \frac{1}{\sqrt{12}}\cdot\frac{\sin\theta}{\Delta_{B_A_+}}\mathrm{Im}(l_z^{ba})(d_x^{ib}d_y^{ia} - d_y^{ib}d_x^{ia})
\end{aligned}$$

with $\sin\theta = \lambda = [\langle C_i^a|(e^2/r_{12})|D_i^a\rangle]/[\Delta E(C_i^a - D_i^a)]$ (vide supra) and $\cos\theta = (1-\lambda^2)^{1/2} \cong 1$ for $\theta \approx 0$.[42]

Electronic transitions into the A_+ state exhibit only very weak MCD C-term intensity in view of the fact that the first contribution is zero and $\Delta_{B\_A_+} = E_{B\_} - E_{A_+}$ is large (Figure 8). This, of course, might have been anticipated as the A_+ excited state mainly contains the D_i^a trip-doublet state. which is not accessible by electronic dipole transitions (vide supra).

$$A \rightarrow J = A\_, \quad K = B_+,\ B\_$$

$$\begin{aligned}
\frac{\Delta\varepsilon}{E} &\sim -\frac{\bar{L}_z^{B_+A_}}{\Delta_{B_+A_}}(\vec{D}_x^{AB_+}\vec{D}_y^{AA_} - \vec{D}_y^{AB_+}\vec{D}_x^{AA_}) \\
&\quad - \frac{\bar{L}_z^{B_A_}}{\Delta_{B_A_}}(\vec{D}_x^{AB_}\vec{D}_y^{AA_} - \vec{D}_y^{AB_}\vec{D}_x^{AA_})
\end{aligned}$$

dx.doi.org/10.1021/ic300201t | Inorg. Chem. 2012, 51, 5748–5763

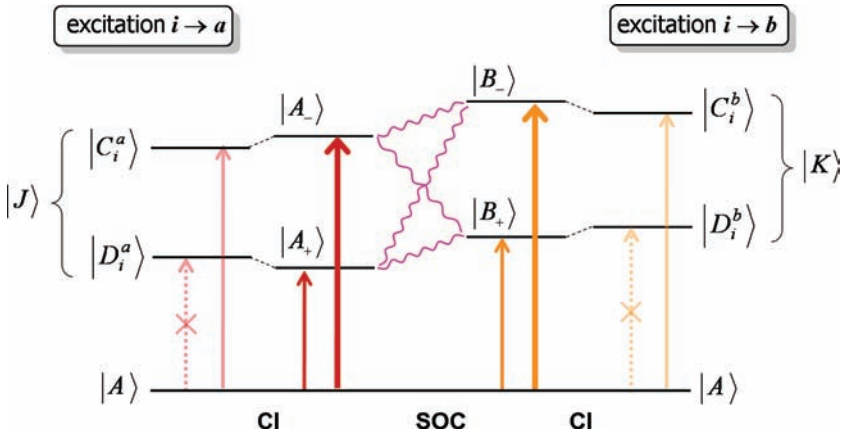

Figure 8. For type III electronic transitions, excited states split into sing-doublet and trip-doublet states. Because spin−orbit coupling vanishes among two sing-doublet states and trip-doublet states are not accessible by electronic dipole transitions, only CI between the sing-doublet and trip-doublet excited states provides a mechanism that gives rise to a nonzero MCD *C*-term intensity. The prevailing contributions are the $A \rightarrow A_-$ and $A \rightarrow B_-$ transitions.

$$\frac{\Delta\varepsilon}{E} \sim -\frac{1}{\Delta_{B_+A_-}}\left(-\frac{1}{\sqrt{12}}(\cos^2\theta - \sin^2\theta) - \frac{2}{3}\sin\theta\cos\theta\right)\mathrm{Im}(l_z^{ba})\cos\theta\sin\theta \times (d_x^{ib}d_y^{ia} - d_y^{ib}d_x^{ia}) - \frac{1}{\Delta_{B_-A_-}}\left(\frac{1}{\sqrt{3}}\sin\theta\cos\theta + \frac{2}{3}\sin^2\theta\right)\mathrm{Im}(l_z^{ba})\cos^2\theta(d_x^{ib}d_y^{ia} - d_y^{ib}d_x^{ia})$$

$$\cong -\frac{1}{\sqrt{12}}\left(2\frac{1}{\Delta_{B_-A_-}} - \frac{1}{\Delta_{B_+A_-}}\right)\sin\theta \times \mathrm{Im}(l_z^{ba})(d_x^{ib}d_y^{ia} - d_y^{ib}d_x^{ia})$$

$\Delta_{B_-A_-} = E_{B_-} - E_{A_-}$ is small compared to $\Delta_{B_-A_+} = E_{B_-} - E_{A_+}$ (Figure 8). As a consequence, the MCD *C*-term intensity of electronic transitions to the A_- state is much higher than that of the $A \rightarrow A_+$ transitions. This agrees with the fact that the main contribution to the A_- state is the C_i^a sing-doublet excited state being accessible by electronic dipole transitions. Considering the absolute values, $\Delta_{B_-A_-}$ is also small compared to $|\Delta_{B_+A_-}|$. As a consequence, the MCD *C*-term intensity of the $A \rightarrow A_-$ transitions is dominated by spin−orbit coupling between the A_- and B_- states.

$$A \rightarrow J = B_+, \quad K = A_+, \ A_-$$

$$\frac{\Delta\varepsilon}{E} \sim -\frac{\bar{L}_z^{A_+B_+}}{\Delta_{A_+B_+}}(\vec{D}_x^{AA_+}\vec{D}_y^{AB_+} - \vec{D}_y^{AA_+}\vec{D}_x^{AB_+}) - \frac{\bar{L}_z^{A_-B_+}}{\Delta_{A_-B_+}}(\vec{D}_x^{AA_-}\vec{D}_y^{AB_+} - \vec{D}_y^{AA_-}\vec{D}_x^{AB_+})$$

$$\frac{\Delta\varepsilon}{E} \sim -\frac{1}{\Delta_{A_+B_+}}\left(-\frac{1}{\sqrt{3}}\sin\theta\cos\theta + \frac{2}{3}\cos^2\theta\right) \times \mathrm{Im}(l_z^{ab})\sin^2\theta(d_x^{ia}d_y^{ib} - d_y^{ia}d_x^{ib}) - \frac{1}{\Delta_{A_-B_+}} \times \left(-\frac{1}{\sqrt{12}}(\cos^2\theta - \sin^2\theta) - \frac{2}{3}\sin\theta\cos\theta\right) \times \mathrm{Im}(l_z^{ab})\sin\theta\cos\theta(d_x^{ia}d_y^{ib} - d_y^{ia}d_x^{ib}) \cong 0 + \frac{1}{\sqrt{12}}\frac{\sin\theta}{\Delta_{A_-B_+}}\mathrm{Im}(l_z^{ab})(d_x^{ia}d_y^{ib} - d_y^{ia}d_x^{ib})$$

Corresponding to the $A \rightarrow A_+$ transition, the MCD *C*-term intensity of this transition is very weak as well because the first contribution is zero and $\Delta_{A_-B_+}$ is comparatively large (Figure 8).

$$A \rightarrow J = B_-, \quad K = A_+, \ A_-$$

$$\frac{\Delta\varepsilon}{E} \sim -\frac{\bar{L}_z^{A_+B_-}}{\Delta_{A_+B_-}}(\vec{D}_x^{AA_+}\vec{D}_y^{AB_-} - \vec{D}_y^{AA_+}\vec{D}_x^{AB_-}) - \frac{\bar{L}_z^{A_-B_-}}{\Delta_{A_-B_-}}(\vec{D}_x^{AA_-}\vec{D}_y^{AB_-} - \vec{D}_y^{AA_-}\vec{D}_x^{AB_-})$$

$$\frac{\Delta\varepsilon}{E} \sim -\frac{1}{\Delta_{A_+B_-}}\left(-\frac{1}{\sqrt{12}}(\cos^2\theta - \sin^2\theta) - \frac{2}{3}\sin\theta\cos\theta\right) \times \mathrm{Im}(l_z^{ab})\cdot\sin\theta\cos\theta\cdot(d_x^{ia}d_y^{ib} - d_y^{ia}d_x^{ib}) - \frac{1}{\Delta_{A_-B_-}} \times \left(\frac{1}{\sqrt{3}}\sin\theta\cos\theta + \frac{2}{3}\sin^2\theta\right)\mathrm{Im}(l_z^{ab})\cos^2\theta(d_x^{ia}d_y^{ib} - d_y^{ia}d_x^{ib}) \cong -\frac{1}{\sqrt{12}}\left(2\frac{1}{\Delta_{A_-B_-}} - \frac{1}{\Delta_{A_+B_-}}\right)\sin\theta \times \mathrm{Im}(l_z^{ab})(d_x^{ia}d_y^{ib} - d_y^{ia}d_x^{ib})$$

Corresponding to the transition to the A_- state, the MCD *C*-term intensity of the $A \rightarrow B_-$ transition is also much higher than that of the $A \rightarrow B_+$ transition. As expected,

dx.doi.org/10.1021/ic300201t | *Inorg. Chem.* 2012, 51, 5748−5763

it is also dominated by spin−orbit coupling between the A_- and B_- states, as $|\Delta E_{(A_- - B_-)}| \ll |\Delta E_{(A_+ - B_-)}|$, considering the absolute values (Figure 8).

In summary, it has to be concluded that, in the case of type III electronic transitions, only CI between the sing-doublet and trip-doublet excited states provides a mechanism that gives rise to a nonzero MCD *C*-term intensity. Multideterminant expressions therefore have to be used to correctly describe the excited states. The $A \rightarrow A_-$ and $A \rightarrow B_-$ transitions are the leading contributions because they have the largest coefficients and are dependent on $1/(\Delta_{B\_A\_})$ and $1/(\Delta_{A\_B\_})$, respectively, with $\Delta_{B\_A\_}$ and $|\Delta_{A\_B\_}|$ being comparatively small. Moreover, these two transitions have opposite signs, giving rise to a *pseudo-A* term (see below). Assuming that the energy difference between the sing-doublet and trip-doublet excited states is large, i.e., in the range of several thousand wavenumbers, the $A \rightarrow A_+$ and $A \rightarrow B_+$ transitions would be expected in the NIR region of the MCD spectra. However, they would show significantly lower intensities compared to the $A \rightarrow A_-$ and $A \rightarrow B_-$ transitions. Moreover, the *C*-term intensities of the $A \rightarrow A_+$ and $A \rightarrow B_+$ transitions show the same signs and therefore do *not* give rise to a *pseudo-A* term.

For further interpretation, it should be noted that the *C*-term intensities of the type III transitions considered in this paper are reduced compared to the *C*-term intensities observed for type I or type II transitions of identical orbital character by a factor of $1/\sqrt{3}\sin\theta$, where $\sin\theta$ is the CI mixing coefficient between sing-doublet and trip-doublet states. Moreover, the actual *C*-term intensity of a type III electronic transition is weakened by the contribution of the second, less important pathway arising from the second possibility of spin−orbit coupling ($A_- \leftrightarrow B_+$ and $A_+ \leftrightarrow B_-$). Finally, slightly different intensities are expected for the $A \rightarrow A_-$ (A_+) and the $A \rightarrow B_-$ (B_+) transitions as $|\Delta_{B_+A_-}| = |E_{B_+} - E_{A_-}| \neq |\Delta_{A_+B_-}| = |E_{A_+} - E_{B_-}|$, which leads to slight asymmetries in the resulting *pseudo-A* terms.

Assignment of the "Double *Pseudo-A* Term" in the MCD Spectrum of [Mo(O)Cl_3dppe]. Considering the "double *pseudo-A* term" feature in the MCD spectrum of [Mo(O)Cl_3dppe], the assignment to the $p_{\text{out-of-plane}}(a,s) \rightarrow d_{yz}, d_{xz}$ LMCT transitions has already been suggested. This assignment is now confirmed based on the derived equations of the MCD *C*-term intensity by determining the MCD signs of the individual transitions from the corresponding transition densities. On the basis of the calculated MO scheme (Figure 5), MO 109/113 and MO 118/119 are the MOs under consideration.

Because the donor orbitals (i) are ligand orbitals and the acceptor orbitals (a) as well as the singly occupied d_{xy} orbital (o) are metal d orbitals, the one-center exchange integral K_{ao} is larger than the two-center exchange integral K_{io}:

$$K_{ao} > K_{io}$$

The mixing coefficient $\sin\theta$ therefore is positive throughout the following expressions (vide supra).

The transition-dipole moments of the individual transitions are determined from the corresponding transition densities (Figure 9). Note that the only contribution to the transition-dipole moments arises from the ligand parts of the considered MOs. The transition densities along x and y have a fixed-phase relationship (either + or −) with the corresponding transition-dipole moments (which appear in the theoretical formulas). However, because the product of two dipole moments enters the formula for the MCD intensity, we do not have to deal with this issue.

Beginning with the $p_{\text{out-of-plane}}(s) \rightarrow d_{yz}, d_{xz}$ transitions ($i \rightarrow a, b$), the $p_{\text{out-of-plane}}(s) \rightarrow d_{yz}$ transition ($i \rightarrow a$, MO 113 → MO 118) is y-polarized in the negative direction, while the $p_{\text{out-of-plane}}(s) \rightarrow d_{xz}$ ($i \rightarrow b$, MO 113 → MO 119) is x-polarized in the negative direction (Figure 9).

As a consequence, the MCD *C*-term intensity of the $p_{\text{out-of-plane}}(s) \rightarrow d_{yz}$ ($A \rightarrow A_-$) transition is positive:

$$\begin{aligned}\frac{\Delta\varepsilon}{E} &\sim -\frac{1}{\sqrt{12}}\left(2\frac{1}{\Delta_{B\_A\_}} - \frac{1}{\Delta_{B_+A\_}}\right)\sin\theta\ \mathrm{Im}(l_z^{ba})\ (d_x^{ib}d_y^{ia} - d_y^{ib}d_x^{ia})\\ &= -\frac{1}{\sqrt{12}}\left(2\frac{1}{\Delta_{B\_A\_}} - \frac{1}{\Delta_{B_+A\_}}\right)\sin\theta\ \mathrm{Im}(\langle xz|l_z|yz\rangle)\\ &\quad\times\{\langle p_\pi(s)|\mu_x|xz\rangle\langle p_\pi(s)|\mu_y|yz\rangle - \langle p_\pi(s)|\mu_y|xz\rangle\langle p_\pi(s)|\mu_x|\psi_a\rangle\}\\ &= -\frac{1}{\sqrt{12}}\left(2\frac{1}{\Delta_{B\_A\_}} - \frac{1}{\Delta_{B_+A\_}}\right)\sin\theta\ (-1)\{(-1)|\langle p_\pi(s)|\mu_x|xz\rangle|(-1)\\ &\quad\times|\langle p_\pi(s)|\mu_y|yz\rangle| - 0\} > 0\end{aligned}$$

because $\Delta_{B\_A\_} = E_{B\_} - E_{A\_} = E_{xz} - E_{yz} > 0$ and $|\Delta_{B_+A\_}|$ is comparatively large.

The MCD *C*-term intensity of the $p_{\text{out-of-plane}}(s) \rightarrow d_{xz}$ ($A \rightarrow B_-$) transition, in contrast, has a negative sign:

$$\begin{aligned}\frac{\Delta\varepsilon}{E} &\sim -\frac{1}{\sqrt{12}}\left(2\frac{1}{\Delta_{A\_B\_}} - \frac{1}{\Delta_{A_+B\_}}\right)\sin\theta\ \mathrm{Im}(l_z^{ab})(d_x^{ia}d_y^{ib} - d_y^{ia}d_x^{ib})\\ &= -\frac{1}{\sqrt{12}}\left(2\frac{1}{\Delta_{A\_B\_}} - \frac{1}{\Delta_{A_+B\_}}\right)\sin\theta\ \mathrm{Im}(\langle yz|l_z|xz\rangle)\\ &\quad\times\{\langle p_\pi(s)|\mu_x|yz\rangle\langle p_\pi(s)|\mu_y|xz\rangle - \langle p_\pi(s)|\mu_y|yz\rangle\langle p_\pi(s)|\mu_x|xz\rangle\}\\ &= -\frac{1}{\sqrt{12}}\left(2\frac{1}{\Delta_{A\_B\_}} - \frac{1}{\Delta_{A_+B\_}}\right)\sin\theta\ (+1)\\ &\quad\times\{0 - (-1)|\langle p_\pi(s)|\mu_y|yz\rangle|(-1)|\langle p_\pi(s)|\mu_x|xz\rangle|\} < 0\end{aligned}$$

with $\Delta_{A\_B\_} = E_{A\_} - E_{B\_} = E_{yz} - E_{xz} < 0$ and $|\Delta_{A_+B\_}|$ being comparatively large.

The $p_{\text{out-of-plane}}(s) \rightarrow d_{yz}, d_{xz}$ transitions thus result in a negative *pseudo-A* term and are now definitely assigned to the MCD bands 3 and 4 at 24800 and 29600 cm^{-1}. They correspond to the observed shoulders at 25000 cm^{-1} (band D) and 30000 cm^{-1} (band E) in the UV/vis spectrum.

The transition-dipole moments for the $p_{\text{out-of-plane}}(a) \rightarrow d_{yz}, d_{xz}$ ($i \rightarrow a, b$) transitions are determined the same way. The $p_{\text{out-of-plane}}(a) \rightarrow d_{yz}$ transition ($i \rightarrow a$, MO 109 → MO 118) then is x-polarized in the positive direction, and the $p_{\text{out-of-plane}}(a) \rightarrow d_{xz}$ transition ($i \rightarrow b$, MO 109 → MO 119) is y-polarized in the positive direction (Figure 9). This results in a negative MCD *C*-term intensity for the $p_{\text{out-of-plane}}(a) \rightarrow d_{yz}$ ($A \rightarrow A_-$) transition:

$$\begin{aligned}\frac{\Delta\varepsilon}{E} &\sim -\frac{1}{\sqrt{12}}\left(2\frac{1}{\Delta_{B\_A\_}} - \frac{1}{\Delta_{B_+A\_}}\right)\sin\theta\ \mathrm{Im}(l_z^{ba})(d_x^{ib}d_y^{ia} - d_y^{ib}d_x^{ia})\\ &= -\frac{1}{\sqrt{12}}\left(2\frac{1}{\Delta_{B\_A\_}} - \frac{1}{\Delta_{B_+A\_}}\right)\sin\theta\ \mathrm{Im}(\langle xz|l_z|yz\rangle)\\ &\quad\times\{\langle p_\pi(a)|\mu_x|xz\rangle\langle p_\pi(a)|\mu_y|yz\rangle - \langle p_\pi(a)|\mu_y|xz\rangle\langle p_\pi(a)|\mu_x|\psi_a\rangle\}\\ &= -\frac{1}{\sqrt{12}}\left(2\frac{1}{\Delta_{B\_A\_}} - \frac{1}{\Delta_{B_+A\_}}\right)\sin\theta\ (-1)\\ &\quad\times\{0 - (+1)|\langle p_\pi(a)|\mu_y|xz\rangle|(+1)|\langle p_\pi(a)|\mu_x|\psi_a\rangle|\} < 0\end{aligned}$$

dx.doi.org/10.1021/ic300201t | *Inorg. Chem.* 2012, 51, 5748−5763

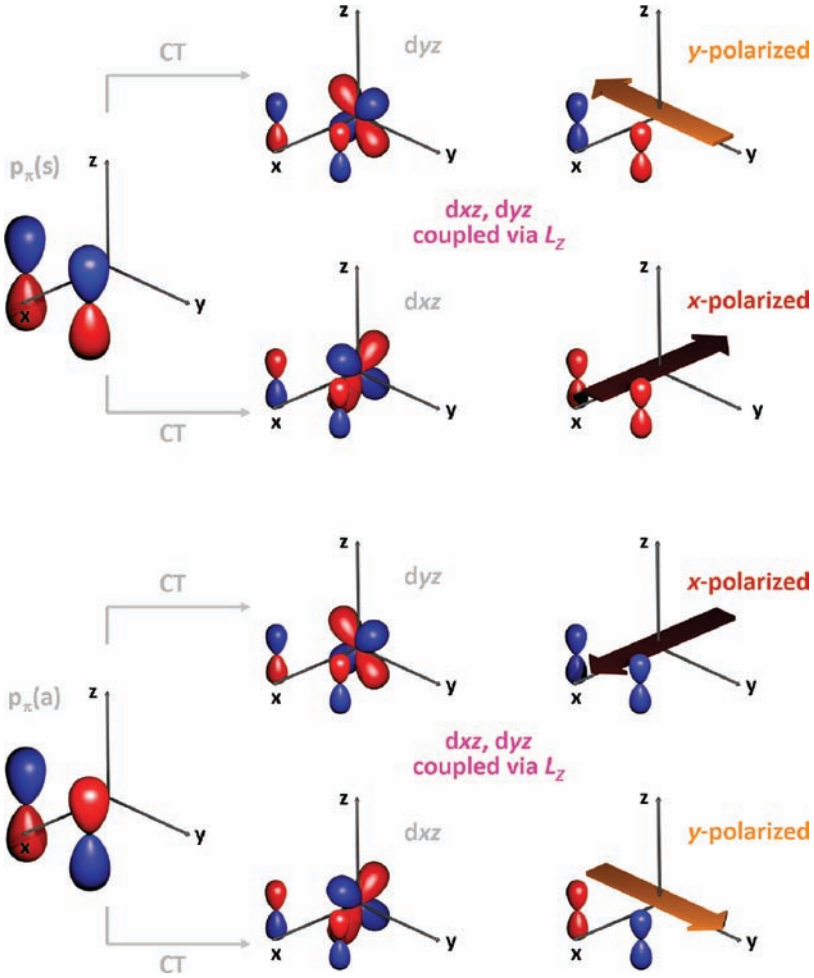

Figure 9. Transition-dipole moments of the $p_{out\text{-}of\text{-}plane}(s,a) \rightarrow d_{yz}$, d_{xz} transitions determined from the considered transition densities.

while the MCD *C*-term intensity of the $p_{out\text{-}of\text{-}plane}(a) \rightarrow d_{xz}$ ($A \rightarrow B_-$) transition is positive:

$$\frac{\Delta\varepsilon}{E} \sim -\frac{1}{\sqrt{12}}\left(2\frac{1}{\Delta_{A_-B_-}} - \frac{1}{\Delta_{A_+B_-}}\right)\sin\theta\ \mathrm{Im}(l_z^{ab})(d_x^{ia}d_y^{ib} - d_y^{ia}d_x^{ib})$$

$$= -\frac{1}{\sqrt{12}}\left(2\frac{1}{\Delta_{A_-B_-}} - \frac{1}{\Delta_{A_+B_-}}\right)\sin\theta\ \mathrm{Im}(\langle yz|l_z|xz\rangle) \times \{\langle p_\pi(a)|\mu_x|yz\rangle\langle p_\pi(a)|\mu_y|xz\rangle - \langle p_\pi(a)|\mu_y|yz\rangle\langle p_\pi(a)|\mu_x|xz\rangle\}$$

$$= -\frac{1}{\sqrt{12}}\left(2\frac{1}{\Delta_{A_-B_-}} - \frac{1}{\Delta_{A_+B_-}}\right)\sin\theta\ (+1) \times \{(+1)|\langle p_\pi(a)|\mu_x|yz\rangle|(+1)|\langle p_\pi(a)|\mu_y|xz\rangle| - 0\} > 0$$

Taken together, the $p_{out\text{-}of\text{-}plane}(a) \rightarrow d_{yz}$, d_{xz} transitions thus lead to a positive *pseudo-A* term and are therefore definitely assigned to the MCD bands 5 and 6 at 30600 and 34100 cm^{-1}, which correspond to the absorption shoulders at 30000 cm^{-1} (band E, together with the MCD band 4) and 34000 cm^{-1} (band F) in the UV/vis spectrum.

The assignment of the "double *pseudo-A*-term" feature in the MCD spectrum of [Mo(O)Cl_3dppe] to the $p_{out\text{-}of\text{-}plane}(s,a) \rightarrow d_{yz}$, d_{xz} LMCT transitions is depicted in Figure 10. Note that it is in agreement with the literature. In the MCD spectrum of various [Mo(O)L(1,2-dithiolate)] [L = hydrotris(3,5-dimethyl-1-pyrazolyl)borate], a negative−positive−positive−negative pattern of MCD bands between 20000 and 30000 cm^{-1} had already been interpreted as LMCT from the symmetric and antisymmetric out-of-plane p_π orbitals of the dithiolate ligands to d_{xz} and d_{yz}.[2,9] The symmetric and antisymmetric p_π orbitals and also the d_{xz} and d_{yz} orbitals are inverted in energy in the case of the [Mo(O)L(1,2-dithiolate)] complexes compared to [Mo(O)-Cl_3dppe]. This leads to the observed inversion of signs within the "double *pseudo-A*-term" feature, which are determined by the symmetry of the donor orbitals.[1]

In the case of the title complex [Mo(O)Cl_3dppe], LMCT transitions from the bonding equivalent of the $p_{out\text{-}of\text{-}plane}(s)$ orbital (MO 103) to the d_{yz} and d_{xz} orbitals should result in another negative *pseudo-A* term at significantly higher energies (>35000 cm^{-1}), which was out of range in the MCD measurements. Theoretically, two very weak transitions arising from the corresponding $A \rightarrow A_+$ and $A \rightarrow B_+$ excitations would additionally be expected in the NIR region of the MCD spectrum.

Additionally, it should be noted that the MCD *C*-term intensities of the $p_{out\text{-}of\text{-}plane}(s,a) \rightarrow d_{yz}$, d_{xz} LMCT transitions (bands 3−6) are lower compared to the intensity of the $p_{in\text{-}plane}(a) \rightarrow x^2 - y^2$ transition (band 1; Figure 4), which confirms that the *C*-term intensities of type III electronic transitions are reduced compared to the *C*-term intensities observed for type I (or type II) transitions of identical orbital character (vide supra).

dx.doi.org/10.1021/ic300201t | *Inorg. Chem.* 2012, 51, 5748−5763

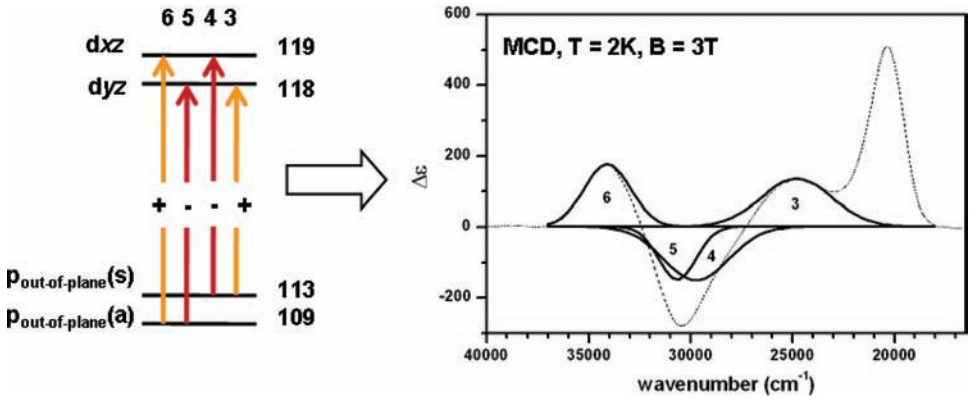

Figure 10. Analysis of the "double *pseudo-A*-term" feature in the low-temperature MCD spectrum of [Mo(O)Cl_3dppe] from MO considerations.

CONCLUSIONS

In the preceding sections, the molybdenum(V) complex [Mo(O)Cl_3dppe] has been investigated with respect to its electronic structure and its spectroscopic properties. Because this complex only has a single electron and exhibits clear C_S symmetry it turned out to be an excellent system for a combined study on the electronic structure using UV/vis and MCD spectroscopy, including determination of the *C*-term signs of the individual electronic transitions. From the DFT calculation of the MOs, the metal and ligand character of the individual MOs could clearly be determined, and on that basis, some trends considering the types and energies of the electronic transitions could be derived from the TDDFT calculations.

The UV/vis absorption band B at 20500 cm^{-1}, which corresponds to the MCD band 1, has been assigned to the $p_{in\text{-}plane}(a) \rightarrow d_{x^2-y^2}$ LMCT transition. This assignment was supported by resonance Raman measurements and the calculated UV/vis spectrum (TDDFT). The most prominent feature of the MCD spectra are two corresponding *pseudo-A* terms between 22000 and 35000 cm^{-1}, giving rise to a "double *pseudo-A* term". From MO considerations, the two *pseudo-A* terms were assigned to the $p_{out\text{-}of\text{-}plane}(s,a) \rightarrow d_{yz}$, d_{xz} LMCT transitions.

In order to evaluate the MCD *C*-term intensity of these transitions, the multideterminant character of the excited states was explicitly considered.[1,20,42] In this way, a treatment for the MCD *C*-term intensity of type III electronic transitions has been developed, which has been missing so far. Importantly, this ensures the general applicability of the C-term expressions of Neese and Solomon to *all* types of ligand-field and charge-transfer transitions of $S = {}^1/_2$ systems and also indicates, in principle, how to handle multideterminant excited states for systems with $S > {}^1/_2$.[1] In the case of type III transitions of $S = {}^1/_2$ systems, CI between the sing-doublet and trip-doublet excited states has been identified to provide the only mechanism giving rise to nonzero MCD *C*-term intensities. For the title complex, the absolute signs of the individual transitions were directly determined from the corresponding transition densities based on the calculated MOs. This protocol thus is also generally applicable and does not depend on particular symmetry properties. Further applications to MCD spectra of systems exhibiting type III transitions are anticipated.

ASSOCIATED CONTENT

Supporting Information

Cartesian coordinates for the DFT energy-minimized complex geometry of [Mo(O)Cl_3dppe] (Table S1). This material is available free of charge via the Internet at http://pubs.acs.org.

AUTHOR INFORMATION

Corresponding Author

*E-mail: ftuczek@ac.uni-kiel.de. Phone: +49 431 880-1410. Fax +49 431 880-1520.

Notes

The authors declare no competing financial interest.

ACKNOWLEDGMENTS

The present work was financially supported by the federal state of Schleswig-Holstein. P.K. acknowledges a Liebig fellowship by Fonds der Chemischen Industrie.

REFERENCES

(1) Neese, F.; Solomon, E. I. *Inorg. Chem.* **1999**, *38*, 1847−1865.
(2) Carducci, M. D.; Brown, C.; Solomon, E. I.; Enemark, J. H. *J. Am. Chem. Soc.* **1994**, *116*, 11856−11868.
(3) Gamelin, D. R.; Kirk, M. L.; Stemmler, T. L.; Pal, S.; Armstrong, W. H.; Pennerhahn, J. E.; Solomon, E. I. *J. Am. Chem. Soc.* **1994**, *116*, 2392−2399.
(4) Solomon, E. I.; Pavel, E. G.; Loeb, K. E.; Campochiaro, C. *Coord. Chem. Rev.* **1995**, *144*, 369−460.
(5) Farrar, J. A.; Neese, F.; Lappalainen, P.; Kroneck, P. M. H.; Saraste, M.; Zumft, W. G.; Thomson, A. J. *J. Am. Chem. Soc.* **1996**, *118*, 11501−11514.
(6) Neese, F.; Solomon, E. I. *J. Am. Chem. Soc.* **1998**, *120*, 12829−12848.
(7) Gamelin, D. R.; Randall, D. W.; Hay, M. T.; Houser, R. P.; Mulder, T. C.; Canters, G. W.; de Vries, S.; Tolman, W. B.; Lu, Y.; Solomon, E. I. *J. Am. Chem. Soc.* **1998**, *120*, 5246−5263.
(8) Brunold, T. C.; Gamelin, D. R.; Stemmler, T. L.; Mandal, S. K.; Armstrong, W. H.; Penner-Hahn, J. E.; Solomon, E. I. *J. Am. Chem. Soc.* **1998**, *120*, 8724−8738.
(9) Inscore, F. E.; McNaughton, R.; Westcott, B. L.; Helton, M. E.; Jones, R.; Dhawan, I. K.; Enemark, J. H.; Kirk, M. L. *Inorg. Chem.* **1999**, *38*, 1401−1410.
(10) Paulat, F.; Lehnert, N. *Inorg. Chem.* **2008**, *47*, 4963−76.
(11) Johansson, F. B.; Bond, A. D.; Nielsen, U. G.; Moubaraki, B.; Murray, K. S.; Berry, K. J.; Larrabee, J. A.; McKenzie, C. J. *Inorg. Chem.* **2008**, *47*, 5079−5092.
(12) Larrabee, J. A.; Johnson, W. R.; Volwiler, A. S. *Inorg. Chem.* **2009**, *48*, 8822−8829.
(13) Geiger, R. A.; Chattopadhyay, S.; Day, V. W.; Jackson, T. A. *J. Am. Chem. Soc.* **2010**, *132*, 2821−2831.

(14) Chattopadhyay, S.; Geiger, R. A.; Yin, G. C.; Busch, D. H.; Jackson, T. A. *Inorg. Chem.* **2010**, *49*, 7530−7535.
(15) Stephens, P. J. *J. Chem. Phys.* **1970**, *52*, 3489−3516.
(16) Stephens, P. J. *Annu. Rev. Chem. Phys.* **1974**, *25*, 201−232.
(17) Solomon, E. I.; Lever, A. B. P. *Inorganic Electronic Structure and Spectroscopy*; Wiley Interscience: Hoboken, NJ, 2006; Vol. *I*.
(18) Ganyushin, D.; Neese, F. *J. Chem. Phys.* **2008**, *128*, 114117.
(19) Sundararajan, M.; Ganyushin, D.; Ye, S. F.; Neese, F. *Dalton Trans.* **2009**, 6021−6036.
(20) Neese, F. Ph.D. Thesis, Universität Konstanz, Konstanz, Germany, 1997.
(21) Römer, R.; Stephan, G.; Habeck, C.; Hoberg, C.; Peters, G.; Näther, C.; Tuczek, F. *Eur. J. Inorg. Chem.* **2008**, 3258−3263.
(22) Söncksen, L.; Römer, R.; Näther, C.; Peters, G.; Tuczek, F. *Inorg. Chim. Acta* **2011**, *374*, 472−479.
(23) Hernandez-Marin, E.; Seth, M.; Ziegler, T. *Inorg. Chem.* **2010**, *49*, 1566−1576.
(24) Seth, M.; Ziegler, T.; Autschbach, J. *J. Chem. Phys.* **2008**, *129*, 104105.
(25) Butcher, A. V.; Chatt, J. *J. Chem. Soc. A* **1971**, 2356−2358.
(26) Frisch, M. J.; Trucks, G. W.; Schlegel, H. B. S.; G., E.; Robb, M. A.; Cheeseman, J. R.; Montgomery, J. A., Jr.; Vreven, T.; Kudin, K. N.; Burant, J. C.; Millam, J. M.; Iyengar, S. S.; Tomasi, J.; Barone, V.; Mennucci, B.; Cossi, M.; Scalmani, G.; Rega, N.; Petersson, G. A.; Nakatsuji, H.; Hada, M.; Ehara, M.; Toyota, K.; Fukuda, R.; Hasegawa, J.; Ishida, M.; Nakajima, T.; Honda, Y.; Kitao, O.; Nakai, H.; Klene, M.; Li, X.; Knox, J. E.; Hratchian, H. P.; Cross, J. B.; Bakken, V.; Adamo, C.; Jaramillo, J.; Gomperts, R.; Stratmann, R. E.; Yazyev, O.; Austin, A. J.; Cammi, R.; Pomelli, C.; Ochterski, J. W.; Ayala, P. Y.; Morokuma, K.; Voth, G. A.; Salvador, P.; Dannenberg, J. J.; Zakrzewski, V. G.; Dapprich, S.; Daniels, A. D.; Strain, M. C.; Farkas, O.; Malick, D. K.; Rabuck, A. D.; Raghavachari, K.; Foresman, J. B.; Ortiz, J. V.; Cui, Q.; Baboul, A. G.; Clifford, S.; Cioslowski, J.; Stefanov, B. B.; Liu, G.; Liashenko, A.; Piskorz, P.; Komaromi, I.; Martin, R. L.; Fox, D. J.; Keith, T.; Al-Laham, M. A.; Peng, C. Y.; Nanayakkara, A.; Challacombe, M.; Gill, P. M. W.; Johnson, B.; Chen, W.; Wong, M. W.; Gonzalez, C.; Pople, J. A. *Gaussian 03*, revision C.02; Gaussian, Inc.: Wallingford, CT, 2004.
(27) Becke, A. D. *J. Chem. Phys.* **1993**, *98*, 5648−5652.
(28) Lee, C. T.; Yang, W. T.; Parr, R. G. *Phys. Rev. B* **1988**, *37*, 785−789.
(29) Miehlich, B.; Savin, A.; Stoll, H.; Preuss, H. *Chem. Phys. Lett.* **1989**, *157*, 200−206.
(30) Becke, A. D. *Phys. Rev. A* **1988**, *38*, 3098−3100.
(31) Perdew, J. P. *Phys. Rev. B* **1986**, *33*, 8822−8824.
(32) Perdew, J. P. *Phys. Rev. B* **1986**, *34*, 7406−7406.
(33) Dunning, T. H., Jr.; Hay, P. J. In *Modern Theoretical Chemistry*; Schaefer, H. F., III, Ed.; Plenum: New York, 1976.
(34) Hay, P. J.; Wadt, W. R. *J. Chem. Phys.* **1985**, *82*, 270−283.
(35) Hay, P. J.; Wadt, W. R. *J. Chem. Phys.* **1985**, *82*, 299−310.
(36) Wadt, W. R.; Hay, P. J. *J. Chem. Phys.* **1985**, *82*, 284−298.
(37) Allouche, A. R. *J. Comput. Chem.* **2011**, *32*, 174−182.
(38) Levason, W.; McAuliffe, C. A.; Sayle, B. J. *J. Chem. Soc., Dalton Trans.* **1976**, 1177−1181.
(39) Collison, D. *J. Chem. Soc., Dalton Trans.* **1990**, 2999−3006.
(40) Pence, H. E.; Selbin, J. *Inorg. Chem.* **1969**, *8*, 353−358.
(41) Lever, A. B. P. *Inorganic Electronic Spectroscopy*; Elsevier: Amsterdam, The Netherlands, 1986.
(42) Ake, R. L.; Gouterman, M. *Theor. Chim. Acta* **1969**, *15*, 20−42.

dx.doi.org/10.1021/ic300201t | *Inorg. Chem.* 2012, 51, 5748−5763